Plant Physiology®

Plant Physiology, 2025, **197**, kiaf092
https://doi.org/10.1093/plphys/kiaf092
Advance access publication 12 March 2025
Research Article

The transcription factor GmbZIP131 enhances soybean salt tolerance by regulating flavonoid biosynthesis

Xiaoli Ni,[1,†] Yiang Wang,[1,†] Liqiang Dai,[1,†] Kedi Jiang,[1] Shuting Zeng,[1] Yixin Huang,[1] Yiting Zhou,[1] Lihui Duan,[1] Cheng Bian,[1] Qi Liu,[1] Hong Sun,[2] Jinbo Shen,[3,*] Shang Wang,[1,*] Erxu Pi[1,*]

[1]College of Life and Environmental Sciences, Hangzhou Normal University, Hangzhou, China
[2]Institute of Plant Protection and Microbiology, Zhejiang Academy of Agricultural Sciences, Hangzhou, P. R. China
[3]National Key Laboratory for Development and Utilization of Forest Food Resources, Zhejiang A & F University, Hangzhou, China
*Author for correspondence: jshen@zafu.edu.cn (J.S.), wangshang0205@hznu.edu.cn (S.W.), erxupi@hznu.edu.cn (E.P.)
†These authors contributed equally to this work.
The author responsible for distribution of materials integral to the findings presented in this article in accordance with the policy described in the Instructions for Authors (https://academic.oup.com/plphys/pages/General-Instructions) is: Erxu Pi (erxupi@hznu.edu.cn).

Abstract

Detoxifying reactive oxygen species (ROS) that accumulate under saline conditions is crucial for plant salt tolerance. The salt overly sensitive (SOS) pathway functions upstream, while flavonoids act downstream, in ROS scavenging under salt stress. However, the potential crosstalk between the SOS pathway and flavonoids in regulating salt stress responses and the associated mechanisms remain largely unexplored. To assess this possible connection, we investigated the role of the soybean (*Glycine max*) transcription factor GmbZIP131 in enhancing salt tolerance by modulating ROS homeostasis through flavonoid biosynthesis. GmSOS2 like (GmSOS2L), a key component of the SOS pathway, phosphorylates and activates GmbZIP131, thus promoting *GmICHG* (isoflavone conjugate-specific beta-glucosidase) expression. Metabolic profiling of transgenic soybean lines revealed that GmbZIP131 upregulates the levels of lupiwighteone and its 7-glucoside precursor, likely processed by GmICHG. Furthermore, overexpression of *GmSOS2L*, *GmbZIP131*, or *GmICHG* enhances the accumulation of lupiwighteone and its 7-glucoside precursor, as well as soybean salt stress tolerance. Our findings reveal a GmSOS2L–GmbZIP131–GmICHG signaling cascade that enhances soybean salt tolerance through flavonoid accumulation. This research uncovers a mechanism linking the SOS pathway to flavonoid metabolism, offering insights for improving soybean stress tolerance and advancing the molecular breeding of salt-tolerant varieties.

Introduction

Currently, soybean (*Glycine max*) is becoming one of the most economically important leguminous crops, serving as an indispensable source of plant oil and protein for the burgeoning global population (Liu et al. 2020). However, the productivity and cultivation area of soybean are constrained by various abiotic stresses, especially high salinity (Rasheed et al. 2022). Therefore, it is crucial to elucidate the sophisticated mechanism of salt tolerance in soybean and the subsequent breeding of salt-tolerant varieties.

High salinity inflicts ionic stress in plant cells (van Zelm et al. 2020). To cope with excess Na^+, plants have evolved a calcium-dependent salt overly sensitive (SOS) pathway. In this pathway, the EF hand calcium-binding protein SOS3 senses the salt-induced cytosolic calcium signal, then interacts with and activates the serine/threonine protein kinase SOS2. The activated SOS2 phosphorylates and stimulates the plasma membrane Na^+/H^+ antiporter SOS1 to extrude excessive Na^+ (Zhu 2016). SOS2 serves as the molecular switch of the SOS pathway by phosphorylating SOS3-like calcium-binding proteins to trigger the activation of calcium-binding protein kinases (Du et al. 2011; Zhou et al. 2014). Meanwhile, SOS2 interacts with the 2C protein phosphatase ABI2, which may inactivate SOS2 to maintain its proper activity level (Ohta et al. 2003). As the SOS pathway has been extensively studied, several substrates of SOS2 apart from calcineurin B–like proteins (Luan et al. 2002) have been identified. Among them, CTR1 activates the ethylene signaling (Li et al. 2024), PLT1/2 and RhoGDI1 maintain root growth (Hao et al. 2023; Liu et al. 2023), CAT2 and CAT3 eliminate peroxide (Verslues et al. 2007) during salt responses.

Plant cells, when subjected to salt stress, can initiate a cascade of detrimental oxidative stress, a phenomenon well-documented in the literature (van Zelm et al. 2020). Reactive oxygen species (ROS) encompass a diverse array of molecules and ions produced as byproducts of molecular oxygen (O_2) metabolism within living organisms. This class includes hydrogen peroxide (H_2O_2), superoxide anion ($O_2^{\bullet-}$), singlet oxygen ($^1O_2$), the hydroxyl radical ($HO^{\bullet}$), and a spectrum of organic and inorganic peroxides (Liu and He 2016; Mittler 2017). In plants, ROS are generated in various cellular compartments, such as mitochondria, chloroplasts, and peroxisomes, where they serve pivotal functions in growth, development, immune responses, and adaptation to a range of abiotic stresses (Kadota et al. 2014; Babbar et al. 2021; Mittler et al. 2022). However, the persistent accumulation of ROS within the plant system can lead to detrimental effects. Excessive ROS can induce cellular damage through the peroxidation of lipids, denaturation of proteins, oxidation of carbohydrates, degradation of pigments, and damage to DNA (Møller et al. 2007). To counteract the deleterious effects of ROS, particularly under conditions of salt stress, plants have evolved a sophisticated array of detoxification mechanisms. These mechanisms are predominantly mediated by enzymatic antioxidants, including superoxide dismutase

Received January 14, 2025. Accepted February 10, 2025.

(Takagi et al. 2016), and peroxidase (POD; Suzuki et al. 2013), as well as nonenzymatic antioxidants, such as ascorbic acid, glutathione (Gallé et al. 2021), and flavonoids (Muhlemann et al. 2018).

Flavonoids are a pivotal class of plant secondary metabolites that bolster the antioxidant defenses of plants, thereby equipping them with enhanced resilience to various stressors (Wang et al. 2017, 2020; Alvarez-Rivera et al. 2022; Song et al. 2022). A wealth of research has underscored the substantial role of bZIP transcription factors in modulating the biosynthesis of flavonoids and in augmenting salt tolerance (Hartmann et al. 2005; Akagi et al. 2012; Malacarne et al. 2016; An et al. 2017; Vadivel et al. 2021). In *Arabidopsis thaliana*, specific bZIP transcription factors, such as AtbZIP17 and AtbZIP60, exert positive regulatory effects during salt stress responses (Liu et al. 2008; Tang et al. 2012). In contrast, AtbZIP24 and AtbZIP62 negatively regulate within the salt tolerance signaling cascade of Arabidopsis (Yang et al. 2009; Rolly et al. 2020). Similarly, in soybean, the overexpression (OE) of *GmbZIP2* upregulates the expression of genes associated with salt stress, thereby conferring improved salt resistance to transgenic plants (Yang et al. 2020). The heterologous expression of *GmbZIP1*, *GmbZIP44*, *GmbZIP62*, and *GmbZIP78* in Arabidopsis positively modulates the plant's salt tolerance (Gao et al. 2011). The bZIP transcription factor family can be categorized into 13 subfamilies based on sequence similarity and the presence of conserved motifs, designated as A, B, C, D, E, F, G, H, I, J, K, L, and S (Yu et al. 2020). These transcription factors exhibit a preference for binding to DNA sequences that contain an ACGT core, such as the C-box (GACGTC) and G-box (CACGTG) elements (Jakoby et al. 2002).

Our phosphoproteomic analysis of soybean roots under salt treatment, compared with control conditions, revealed an upregulation in the S135 phosphorylation (within the motif HxxS) levels of GmbZIP131. Interestingly, previous research demonstrated that SOS2 predominantly targets substrates for phosphorylation at the bxxS/T motif, where "b" denotes a basic amino acid. Examples of such motifs include RxxS or RxxT, and "S/T" marks the sites targeted for phosphorylation by SOS2 (Gong et al. 2002). The serine residue at position 135 in GmbZIP131 seems like a potential phosphorylation site for the kinase SOS2 or its homologs.

GmbZIP131 is a bZIP transcription factor in soybean, classified within Subfamily I as depicted in Supplementary Fig. S1. Members of this subfamily are recognized for their pivotal roles as regulatory modulators in orchestrating the plant's adaptive responses to a multitude of environmental stressors, including osmotic, cold, and mechanical stress (Yu et al. 2020). However, the detailed biological function of bZIP131 within this context is yet to be fully understood.

This study offers perspective on the molecular dynamics that govern soybean's response to salt stress and reveals the sophisticated crosstalk between flavonoid biosynthesis and the SOS pathway. GmbZIP131 emerges as a central regulatory hub in this network, orchestrating the plant's response under saline conditions.

Results

GmbZIP131 positively regulates soybean tolerance to salinity

To gain initial insights into the biological role of GmbZIP131, we developed transgenic soybean plants with either OE or RNA interference (RNAi)-mediated silencing of *GmbZIP131*, and validated the transcript levels by reverse transcription quantitative PCR (RT-qPCR; Supplementary Fig. S2). Seedlings of these transgenic plants were treated with 200 mM NaCl, compared with wild-type (WT) Tianlong 1#. Results showed that WT, RNAi, and OE plants displayed no phenotypic differences under normal conditions (Fig. 1A). In contrast, OE lines exhibited healthier growth compared with WT and RNAi plants, which displayed more visible damage and withering under salt stress (Fig. 1B). Specifically, the fresh weight of roots in transgenic lines OE-3 (0.952 ± 0.040 g) and OE-5 (0.830 ± 0.036 g) was markedly greater than that observed in the WT plants (0.707 ± 0.048 g), as depicted in Fig. 1C. In contrast, the fresh weight of roots in RNAi lines RNAi-1 (0.586 ± 0.010 g) and RNAi-2 (0.429 ± 0.050 g) was significantly reduced in comparison with the WT. Additionally, GmbZIP131 also exerted a similar regulatory effect on soybean root length. After salt treatment, the root lengths of OE-3 and OE-5 were significantly greater than those of the WT, while the root lengths of RNAi-1 and RNAi-2 were significantly shorter than those of the WT (Supplementary Fig. S3). These results suggested that GmbZIP131 exerts a positive regulatory effect on the salt tolerance of soybean roots. This enhancement of salt tolerance, attributed to GmbZIP131, is similarly evident in both soybean stems (Fig. 1D) and leaves (Fig. 1E). Collectively, these findings confirm that GmbZIP131 positively modulates soybean's tolerance to salt stress.

GmbZIP131 can enhance tolerance to salinity-induced oxidation

Previous research implicate bZIP transcription factors in the mediation of cellular antioxidant mechanisms and osmotic stress responses (Van Leene et al. 2016; Yu et al. 2020; Feng et al. 2021). Building on these findings, we hypothesized that GmbZIP131 could enhance salt tolerance in soybean by bolstering its capacity to withstand osmotic stress and maintaining ROS homeostasis.

Our results indicated no significant disparities in hydrogen peroxide (H_2O_2) levels, POD activity, malondialdehyde (MDA) concentrations, or proline levels among WT, RNAi, and OE plants under nonstressed conditions. After salt treatment, OE plants accumulated the least ROS, as examined by histochemical staining with 3,3′-diaminobenzidine (DAB) and nitro blue tetrazolium (NBT) to indicate in situ accumulation of H_2O_2 and O_2^- (Fig. 2, A and B). These results were further confirmed using quantitative measurement of H_2O_2 content (Fig. 2C). In roots, POD activities were significantly higher in OE lines OE-3 (78.933 ± 0.643 U/g) and OE-5 (77.484 ± 1.293 U/g) compared with WT (68.019 ± 0.488 U/g). In contrast, RNAi-1 (48.600 ± 0.240 U/g) and RNAi-2 (48.311 ± 0.367 U/g) showed significantly lower POD activities than WT (Fig. 2D). Moreover, the MDA content (Fig. 2E) exhibited an inverse correlation with POD activity, whereas the proline level (Fig. 2F) demonstrated a similar trend. These associations were further corroborated by similar trends seen in stems and leaves. These results suggest that GmbZIP131 improves soybean salt tolerance primarily regulating osmotic equilibrium and maintaining ROS homeostasis.

Proteins involved in flavonoid synthesis play important roles in salt responses

To achieve a thorough examination of proteins pivotal to the regulation of osmotic equilibrium and the preservation of ROS homeostasis in soybeans, liquid chromatography-tandem MS (LC–MS/MS) was deployed to scrutinize root samples from WT soybeans under both normal and salt conditions. Results of 3 biological replicates of MS data and quality control (QC) data are

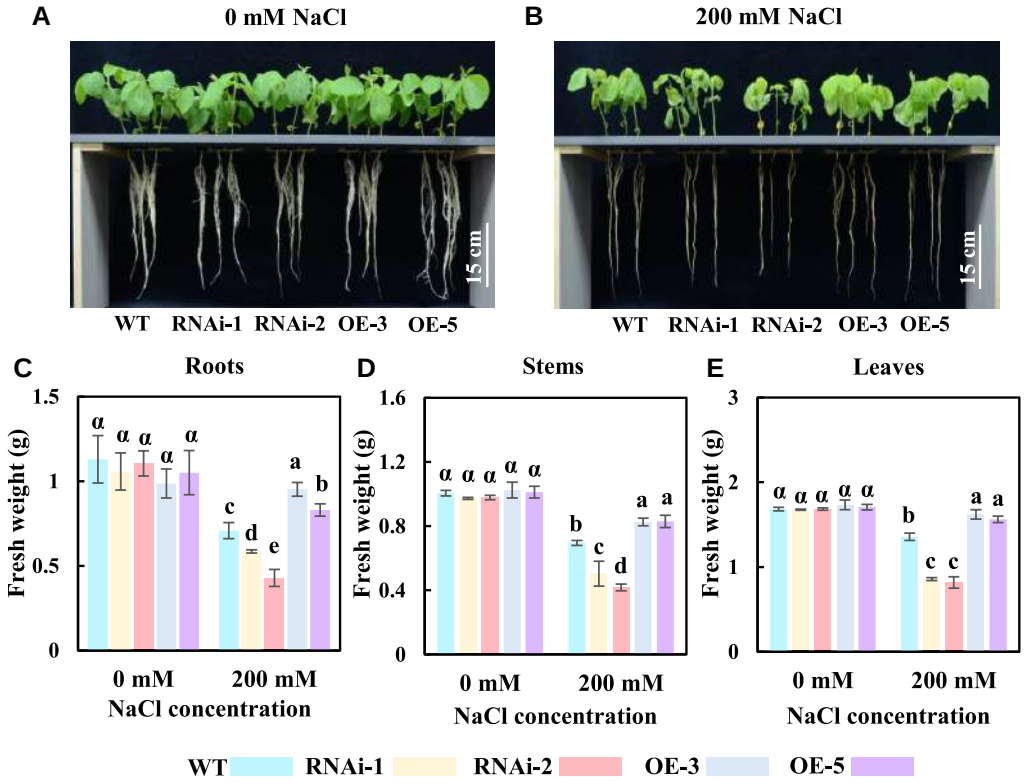

Figure 1. GmbZIP131 enhances salinity tolerance in soybeans. **A** and **B)** Representative phenotypes of WT, *GmbZIP131*-RNAi knockdown (KD) and *GmbZIP131* OE seedlings 24 h after treatment with 200 mM NaCl compared with untreated 1/4-strength Hoagland's solution control. **C** to **E)** Quantification of fresh weights of roots **(C)**, stems **(D)**, and leaves **(E)** in WT, KD, and OE seedlings 24 h postsalt treatment; $n = 3$ independent biological replicates per genotype; data shown as mean ± SD. For all variables with the same letter, the difference between the means is not statistically significant. Different letters indicate statistically significant differences at $P < 0.05$ by 1-way ANOVA followed by Duncan's significant difference test. The experiments presented in **A** and **B** were repeated 3 times with consistent results. **C** to **E)** The labels "0 mM" and "200 mM" on the *x*-axis represent the concentrations of the salt treatment.

included in Supplementary Table S1 and Fig. S4. A total of 14,126 identified proteins and 8,011 quantifiable proteins were detected. In these, 2,487 showed a significant difference with 1,011 upregulated proteins and 1,476 downregulated proteins (Supplementary Fig. S5A). Gene ontology enrichment analysis showed that these differentially expressed proteins were mainly involved in carbohydrate metabolic process, translation, oxidative stress process, and hydrogen peroxide catabolic process (Supplementary Fig. S5B). Kyoto Encyclopedia of Genes and Genomes (KEGG) enrichment analysis showed that the differentially expressed proteins were related to glycosphingolipid biosynthesis-ganglio series, C5-branched dibasic acid metabolism, fatty acid degradation, biosynthesis of secondary metabolites, as well as flavonoid synthesis (Supplementary Fig. S5C).

Given the crucial role of flavonoids as scavengers of ROS in plants under salt stress and the well-documented involvement of bZIPs in regulating flavonoid biosynthesis (Akagi et al. 2012; Malacarne et al. 2016; Yu et al. 2020), we analyzed the expression profiles of proteins associated with the flavonoid biosynthetic pathways. Among the 36 identified proteins related to flavonoid biosynthesis, 10 proteins were significantly upregulated after salt treatment. Particularly, the content of Glyma.12G053800.1.p (isoflavone conjugate-specific beta-glucosidase) was markedly upregulated (Supplementary Fig. S5D and Table S2), indicating that it is induced by salt stress and positively regulates the salt response in soybean.

GmbZIP131 regulates key genes involved in flavonoid biosynthesis

To comprehensively identify downstream targets of GmbZIP131, we conducted RNA sequencing of OE-3 and RNAi-2 roots under the control and salinity conditions. The data quality was sufficient for follow-up analysis (Supplementary Fig. S6 and Tables S3 and S4). The detailed information of RNA-seq data is shown in Supplementary Tables S5 and S6. After NaCl treatment, 12,938 and 12,818 transcripts, respectively, were significantly upregulated and downregulated in OE roots ($P_{adjust} < 0.05$) (Fig. 3A) compared with those under control conditions. Besides, 12,657 and 12,477 transcripts, respectively, were remarkably upregulated and downregulated in RNAi roots ($P_{adjust} < 0.05$; Fig. 3B) after salt stress.

It was noticed that there were 1,750 transcripts whose expression level were significantly higher in OE compared with RNAi after salt treatment, while no significant difference was found in these 2 lines in control conditions. It suggested these genes were probably induced by salinity and under control of GmbZIP131 (Fig. 3C and Supplementary Table S7). KEGG annotation analysis showed that they were mostly involved in metabolic processes and genetic information processing (Fig. 3D). In addition, isoflavone biosynthesis was enriched through KEGG enrichment analysis, as well as glycolysis/gluconeogenesis, terpenoid backbone biosynthesis (Fig. 3E), indicating that GmbZIP131 might participate in these biological processes. Intriguingly, in alignment

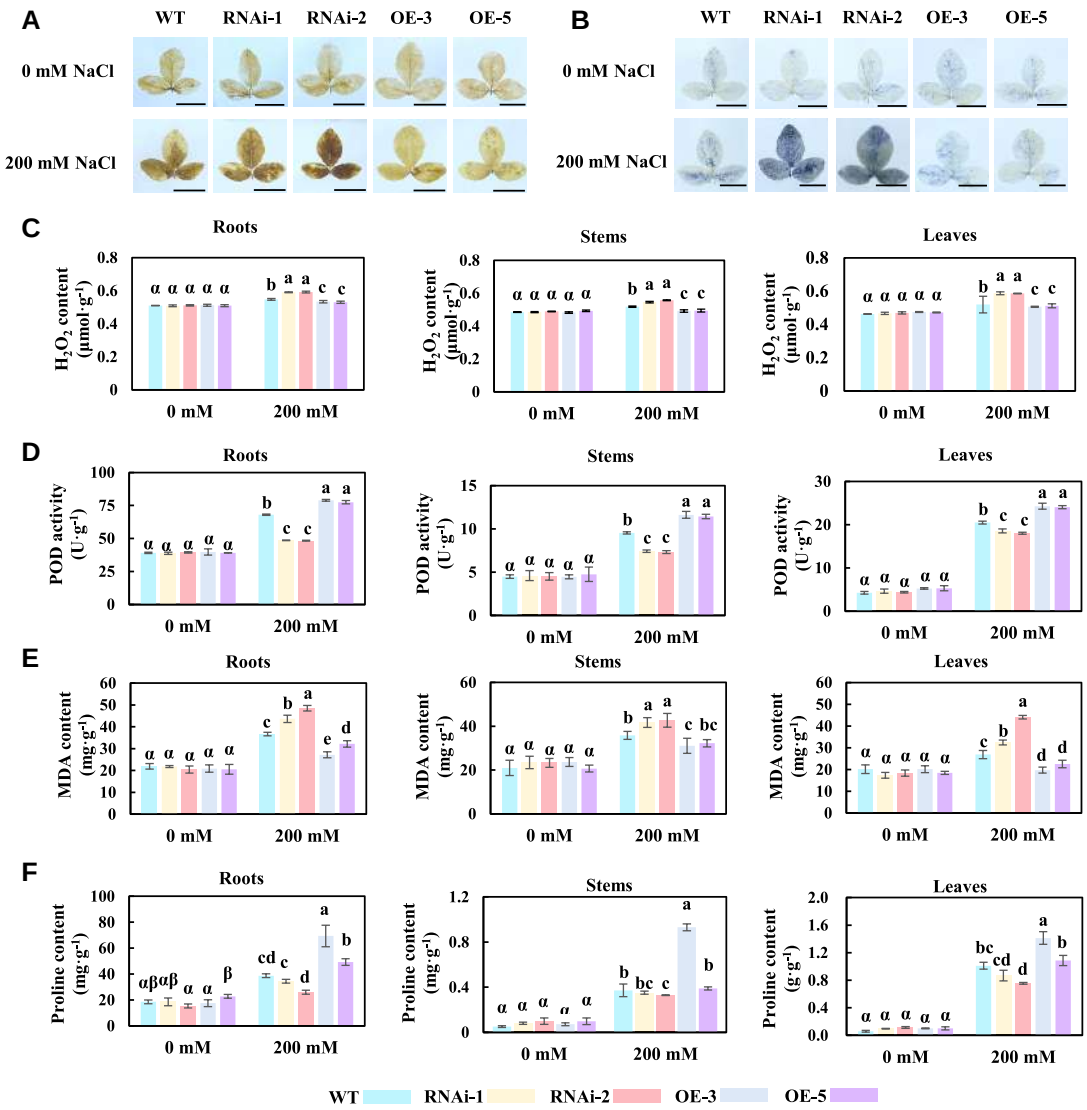

Figure 2. GmbZIP131 regulates ROS homeostasis in soybean under salt stress. **A** and **B)** Visualization of in situ accumulation of **A)** hydrogen peroxide via DAB staining and **B)** superoxide radical via NBT staining in leaves and roots of WT, OE, and RNAi plants in response to 200 mM NaCl treatment compared with untreated controls. Bars = 5 cm. **C** to **F)** Quantification of physiological and biochemical indicators related to oxidative damage and osmotic stress in control and NaCl-treated samples: **C)** H_2O_2 levels, **D)** POD enzymatic activity, **E)** MDA content, and **F)** proline content. All data represent mean ± SD of $n = 3$ independent biological replicates per genotype and treatment; different letters indicate statistically significant differences at $P < 0.05$ by 1-way ANOVA followed by Duncan's significant difference test. The experiments presented in **A** and **B** were repeated 3 times with consistent results. **C** to **F)** The labels "0 mM" and "200 mM" on the x-axis represent the concentrations of the salt treatment.

with the salt-responsive protein profiles identified in the proteomic dataset, the *isoflavone conjugate-specific beta-glucosidase* (*GmICHG*) was notably among these 1,750 transcripts. Consequently, we postulate that *GmICHG* represents a salt-inducible gene that is regulated by GmbZIP131.

To test this hypothesis, we examined *GmICHG* expression levels in roots of WT, OE-3 and RNAi-2 seedlings with or without 200 mM NaCl treatment using RT-qPCR. After salt treatment, the transcriptional expression of *GmICHG* was increased in all 3 plants, especially in OE-3. In the presence of salt, the transcriptional level of *GmICHG* in OE-3 was significantly higher than that in WT ($P = 0.000057$), while its expression level in RNAi-2 was lower than WT ($P = 0.0056$; Fig. 3, F and G). Similar results were obtained in the total flavonoids content of roots (Fig. 3H). Combined with the proteomics results, we hypothesized that *GmICHG* is a target gene of GmbZIP131 and its regulation of *GmICHG* may be in the form of activation induced by salt stress.

GmbZIP131 directly binds to the promoters of the salt-responsive *GmICHG*

Since the function of GmbZIP131 and its subcellular localization have not been previously reported, we transiently expressed a GmbZIP131-GFP fusion protein in *Nicotiana benthamiana* leaves to examine its localization. Fluorescence microscopy showed that the GmbZIP131-GFP fusion protein localized to the nucleus (Fig. 4A). Furthermore, we conducted subcellular fractionation experiments, and the results confirm that GmbZIP131 is exclusively localized in the nucleus, with no detectable presence in the cytoplasm (Supplementary Fig. S7).

To determine whether GmbZIP131 modulates *GmICHG* by directly binding to the promoter of the *GmICHG*, we analyzed its promoter and discovered G-box motifs (CACGTG), the most common targets of bZIPs (Yu et al. 2020). We performed chromatin immunoprecipitation (ChIP) followed by PCR to investigate whether GmbZIP131 binds to the *GmICHG* promoter in planta. Using primer

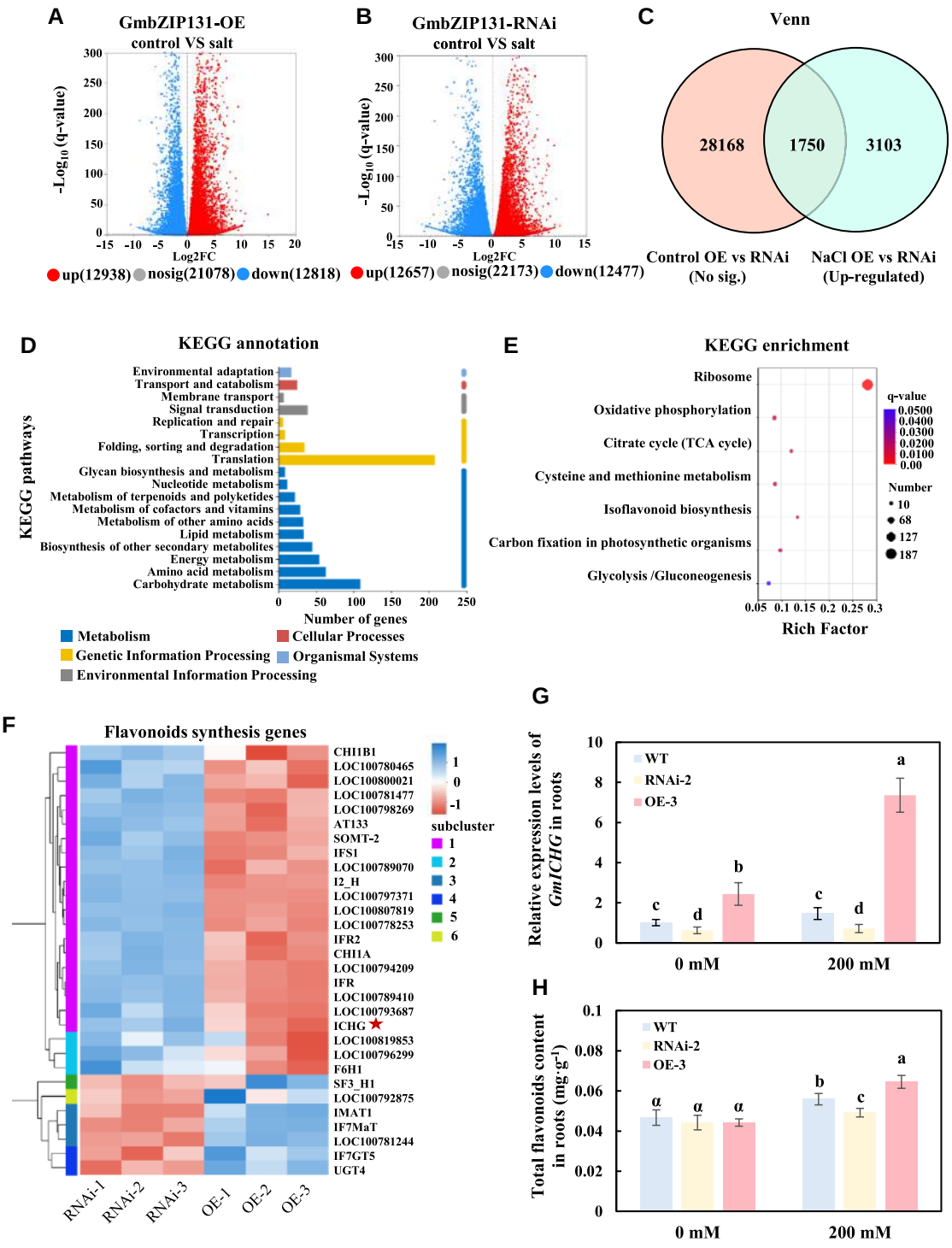

Figure 3. Regulatory roles of GmbZIP131 in key genes involved in flavonoid biosynthesis. **A)** Volcano plot illustrating the DEGs in GmbZIP131-overexpressing soybeans between control and NaCl-treated samples ($P_{adjust} < 0.05$). **B)** Volcano plot displaying the DEGs in GmbZIP131 knockdown soybeans between control and NaCl-treated samples ($P_{adjust} < 0.05$). **C)** Venn diagram depicting the overlap of DEGs upregulated by GmbZIP131 ($P_{adjust} < 0.05$). **D)** Histogram demonstrating the KEGG annotation analysis of DEGs upregulated by GmbZIP131. **E)** KEGG enrichment analysis of DEGs upregulated by GmbZIP131. **F)** Heat map displaying identified DEGs associated with flavonoid biosynthesis. **G)** Transcriptional expression dynamics of *GmICHG* in WT, OE-3, and RNAi-2 roots in response to salt stress. **H)** Variations in flavonoid content among WT, OE-3, and RNAi-2 roots under salt stress. All data represent mean ± SD of $n = 3$ independent biological replicates per genotype and treatment. Different letters indicate statistically significant differences at $P < 0.05$ by 1-way ANOVA followed by Duncan's significant difference test. **G** and **H)** The labels "0 mM" and "200 mM" on the *x*-axis represent the concentrations of the salt treatment.

pair ChIPGmICHG-P1 spanning a 247 bp region of the GmICHG promoter, we detected significant enrichment of this promoter fragment in the ChIP sample from roots expressing 35S::*GmICHG-RFP-HA* compared with the negative control (Fig. 4B). This result confirms the specificity of our ChIP assays and demonstrates in vivo binding of GmbZIP131 to the *GmICHG* promoter in vivo.

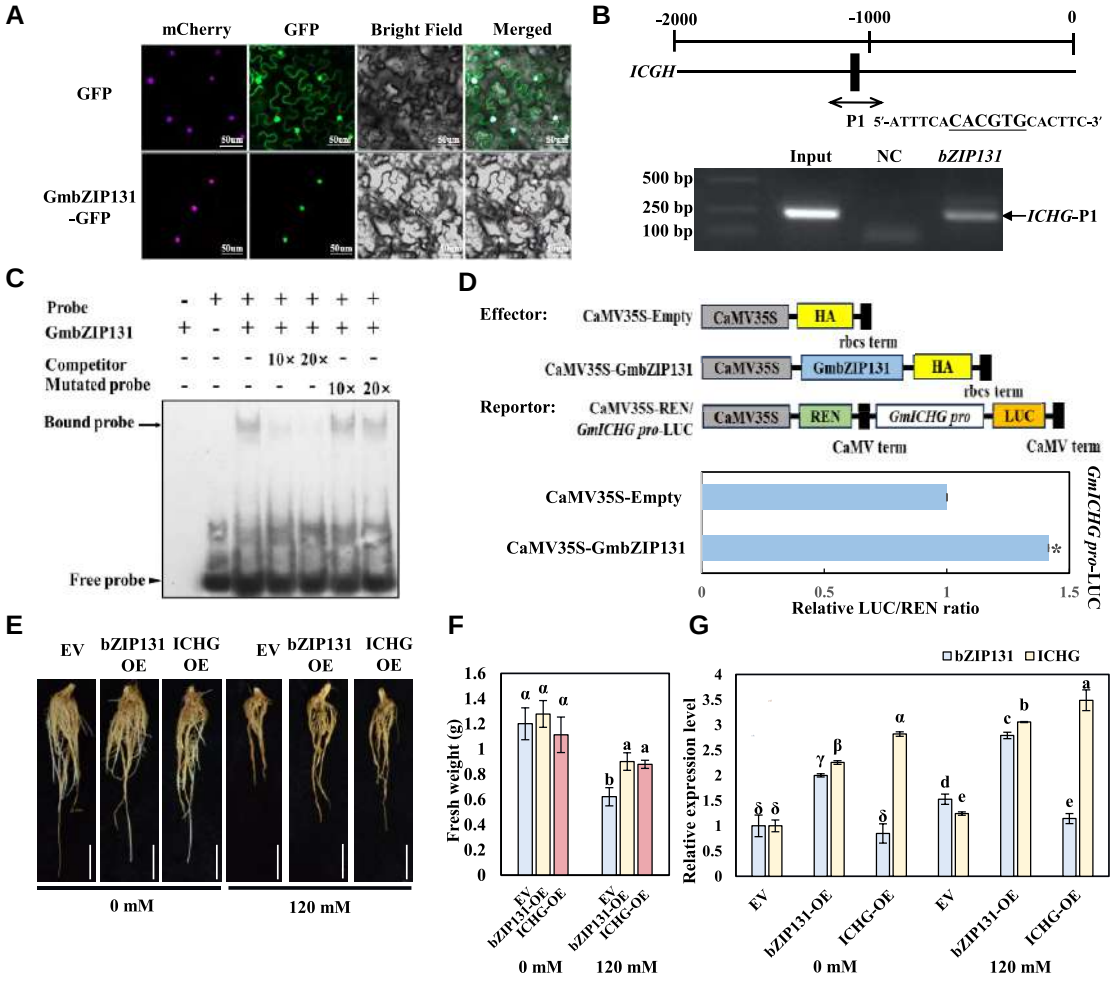

Figure 4. GmbZIP131 directly binds to the promoters of the salt-responsive gene *GmICHG*. **A)** Subcellular localization of GmbZIP131-GFP fusion protein in *N. benthamiana*. The GFP EV was used as a control. The nucleus marker D53-mCherry was used as an indicator for the nucleus (Zhou et al. 2013). Scale bar = 20 μm. **B)** ChIP–PCR assays indicate that GmbZIP131 binds to the promoter regions containing the G-box in vivo. The EV was used as a negative control. GmbZIP131 specifically binds to the *GmICHG* promoter. The underlined sequence represents the G-box *cis*-acting element. **C)** EMSA using affinity-purified fusion protein HIS-GmbZIP131 incubated with biotin-labeled probes of *GmICHG* containing WT or mutated G-box elements. To test specificity, unlabeled competitor DNA carrying either the WT or mutated palindrome was added in 10- or 20-fold molar excess. **D)** The DLR assay verifying GmbZIP131 transactivation activity on *GmICHG* promoter. **E** to **G)** GmbZIP131-mediated regulation of GmICHG potentiates salinity tolerance in soybeans. **E)** Representative phenotypes of hairy roots from EV (*pDL28-DsRed* EV), GmbZIP131-OE (*pDL28-GmbZIP131-DsRed*), and GmICHG-OE (*pDL28-GmICHG-DsRed*) are depicted 7 d posttreatment with 120 mM NaCl, in contrast to the untreated 1/4-strength Hoagland's solution control. Bars = 3 cm. **F)** Quantification of fresh weights of hairy roots in EV, GmbZIP131-OE and GmICHG-OE, hairy roots following 120 mM NaCl salt treatment; $n = 3$ independent biological replicates per genotype; data shown as mean ± SD. Different letters indicate statistically significant differences at $P < 0.05$ by 1-way ANOVA and Student's *t*-test. **G)** Transcriptional expression dynamics of GmbZIP131, *GmICHG* in EV, GmbZIP131, *GmICHG* in GmbZIP131-OE, and GmbZIP131, *GmICHG* in GmICHG-OE hairy roots in response to salt stress; $n = 3$ independent biological replicates per genotype; data shown as mean ± SD. Different letters indicate statistically significant differences at $P < 0.05$ by 1-way ANOVA followed by Duncan's significant difference test. The experiments presented in **A**, **B**, **C**, and **E** were repeated 3 times with consistent results. **E** to **G)** The labels "0 mM" and "200 mM" on the x-axis represent the concentrations of the salt treatment.

To validate the interaction between GmbZIP131 and the *GmICHG* promoter, we performed an electrophoretic mobility shift assay (EMSA) using biotin-labeled probes containing the G-box motif from the *GmICHG* promoter sequence. These probes were incubated with purified GmbZIP131 protein. EMSA results demonstrated specific binding of GmbZIP131 to the WT probe, which was abolished by the addition of excess unlabeled competitor probes but not by mutant probes in which the sequence of the G-box motif was altered to AAAAAA (Fig. 4C). To further explore the relationship of the GmSOS2L, GmbZIP131, and *GmICHG*, we cloned the upstream 2 kb promoter of *GmICHG* and analyzed it by a dual-luciferase reporter (DLR) assay in *N. benthamiana* leaves. As depicted in Fig. 4D, the co-transformation of GmbZIP131 and GmSOS2L exerted a more pronounced activation effect on the promoter sequences of *GmICHG* compared with the effect observed with GmbZIP131 alone. These results suggested that GmbZIP131 is capable of binding to the promoter of *GmICHG*, thereby modulating its transcriptional expression.

To elucidate the roles of GmICHG and GmbZIP131 in conferring salinity tolerance in soybean, we engineered WT soybean plants harboring transgenic hairy roots that overexpress either *GmbZIP131* or *GmICHG*. These constructs were designed to functionally assess their individual contributions to the trait. A parallel set of transgenic lines carrying an empty vector (EV) served as a negative control to distinguish the effects of the candidate genes from baseline responses. This approach allowed us to

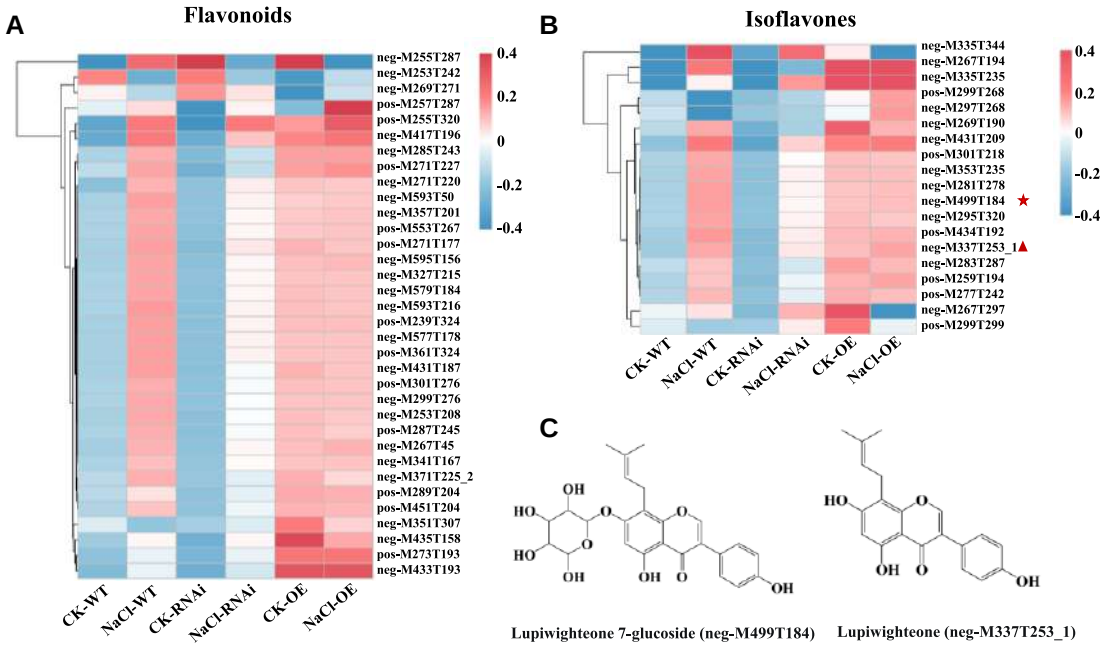

Figure 5. GmbZIP131 orchestrates the accumulation of flavonoids. **A)** Heat map highlighting the metabolites involved in flavonoid biosynthesis. **B)** Heat map illustrating the metabolites associated with isoflavone biosynthesis. Two pentagrams mark the metabolites lupiwighteone and lupiwighteone 7-glucoside. **C)** The molecular structures of lupiwighteone and lupiwighteone 7-glucoside. **A** and **B)** The color scale bar indicates relative abundance levels of flavonoids and isoflavones, respectively.

systematically investigate the potential positive regulatory effects of GmICHG and GmbZIP131 on the soybean's capacity to withstand saline stress. Transgenic hairy roots were selected by red fluorescence (Supplementary Fig. S8). Verified plants with red fluorescent hairy roots were treated hydroponically with 120 mM NaCl. Our investigation exhibited that transgenic soybean hairy roots, with the OE of *GmICHG*, exhibit a significant improvement in salt tolerance compared with those transformed with a control vector lacking the *GmICHG* construct. This notable enhancement underscores the crucial role of *GmICHG* in imparting resilience to saline stress in the soybean root system (Fig. 4, E and F). RT-qPCR analysis demonstrated that the *GmICHG* gene exhibited a significant upregulation in transcriptional abundance within *GmICHG*-overexpressing (GmICHG-OE) roots compared with those transformed with a control EV. Additionally, roots overexpressing *GmbZIP131* (GmbZIP131-OE) showed a pronounced enhancement in the transcriptional activity of the *GmICHG* gene (Fig. 4G).

Under control conditions, the 3 transgenic soybean lines exhibited no significant phenotypic variations, as depicted in Fig. 4F. Upon exposure to salt stress, roots of plants transformed with the EV maintained comparable growth patterns, suggesting that the transformation with an EV did not adversely affect soybean growth and thus could serve as an appropriate control. The inhibitory effects of salt on root growth were least severe in the *GmICHG*-overexpressing (GmICHG-OE) plants, followed by those overexpressing *GmbZIP131* (GmbZIP131-OE), as illustrated in Fig. 4F. Collectively, these findings imply that GmICHG may enhance soybean's salt tolerance in a manner that is dependent on the transactivation activity of GmbZIP131.

GmbZIP131 regulates flavonoid accumulation

Our results suggest that OE of *GmbZIP131* increases total flavonoid accumulation in soybean (Fig. 3H). However, the specific flavonoids involved in salt tolerance remain unknown. To address this, we performed metabolomic analysis to identify flavonoids regulated by GmbZIP131 under salt stress. Roots of WT, OE, and RNAi plants grown under control and saline conditions were collected for metabolite analysis. Each sample had 3 biological replicates. Overlay analysis of QC–total ion current chromatograms and multiple reaction monitoring analysis showed high reproducibility and reliability across replicates (Supplementary Fig. S9), indicating the dataset was suitable for further analysis.

After removing redundant metabolites, a total of 718 metabolites were detected in both negative and positive ionization modes (Supplementary Table S8). Among these, 665 metabolites showed differential accumulation in response to salt treatment. Specifically, 34 metabolites involved in flavonoid biosynthesis (Fig. 5A and Supplementary Table S9) and 19 metabolites involved in isoflavone biosynthesis were differentially accumulated (Fig. 5B and Supplementary Table S10). These results were consistent with the transcriptomic and proteomic data, supporting the significance of the flavonoid and isoflavone biosynthesis pathways in the salt stress response. Six metabolites, including (2S)-liquiritigenin (pos-M257T287), liquiritin (neg-M417T196), norizalpinin (pos-M271T227), 4′-hydroxy-5-methoxyflavone (neg-M267T45), lupiwighteone (neg-M337T253_1), and lupiwighteone 7-glucoside (neg-M499T184), showed increased levels in both WT and genetically modified soybean roots under salt stress (Fig. 5B). The highest levels of these metabolites were observed in overexpressing roots, while the lowest levels were observed in RNAi roots. This suggests that these metabolites may play crucial roles in responses to salt stress regulated by GmbZIP131.

Previous research has demonstrated that GmICHG plays a crucial role in the liberation of free isoflavones from their conjugates with 7-glucoside (Suzuki et al. 2006). Furthermore, a recent study provided evidence that GmICHG is involved in the hydrolysis of the isoflavone glycosides in the root apoplast, leading to increased isoflavone contents in both roots and the rhizosphere soil (Matsuda et al. 2023). Based on these findings, it can be inferred

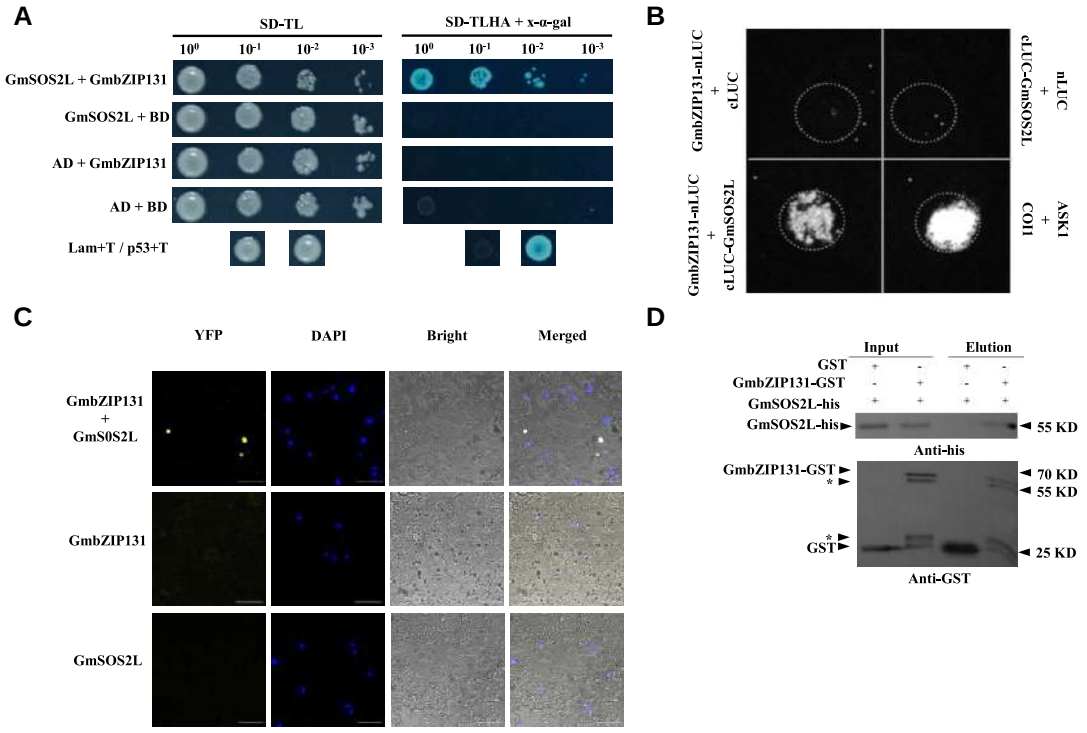

Figure 6. GmbZIP131 interacts with soybean SOS2-like protein kinase GmSOS2L. **A)** Y2H analysis showing physical interaction between GmbZIP131 and GmSOS2L. Serially diluted yeast were plated on SD dropout medium with X-α-gal. AD, activation domain vector; BD, DNA-binding domain vector. **B)** Split-LCI in *N. benthamiana* leaves infiltrated with GmbZIP131-nLUC and GmSOS2L-cLUC fusion constructs. ASK1-cLUC with COI1-nLUC serve as positive control. **C)** BiFC visualized by confocal microscopy confirms the GmbZIP131–GmSOS2L interaction in planta in transfected *N. benthamiana* leaf epidermal cells. DAPI was used as a fluorescent dye to stain the nuclei of cells. Bars = 50 μm. **D)** GST pull-down assay of interaction between GmbZIP131 and GmSOS2L in vitro. The resulting immunoprecipitates were subsequently probed by immunoblotting (IB) using antibodies specific to GST or His-tags. All these experiments were repeated 3 times with consistent results.

that lupiwighteone 7-glucoside (Fig. 5C) acts as a substrate for GmICHG hydrolysis, resulting in the production of lupiwighteone (neg-M337T253_1).

Identification of GmbZIP131 as a substrate of GmSOS2L

GmSOS2L was identified as an interacting partner of GmbZIP131 through screening a salt-induced cDNA library in a yeast 2-hybrid (Y2H) system (Fig. 6A). This interaction was confirmed in planta using split-luciferase complementation imaging (LCI; Fig. 6B), bimolecular fluorescence complementation (BiFC; Fig. 6C), and pull-down assay (Fig. 6D). GmSOS2L/GmPKS4, a protein kinase localized to both the nucleus and cytoplasm, is implicated in enhancing soybean salinity tolerance (Ketehouli et al. 2021). Its transcription is upregulated under saline conditions, and OE in transgenic *A. thaliana* and soybean hairy roots has been shown to augment the scavenging of ROS and bolster the transcriptional regulation of stress-responsive genes (Ketehouli et al. 2021). In alignment with these results, our investigation revealed that transgenic soybean hairy roots (Supplementary Fig. S10), in which *GmSOS2L* was overexpressed, demonstrate a marked improvement in salt tolerance relative to those transformed with a control vector devoid of the *GmSOS2L* construct. This enhancement underscores the pivotal role of GmSOS2L in conferring saline stress resilience in soybean root systems (Supplementary Fig. S11, A and B). Moreover, we observed that the transcriptional levels of the *GmICHG* gene were robustly upregulated in hairy roots of plants overexpressing either *GmSOS2L* or *GmbZIP131*. Notably, salt stress could further amplify this upregulatory effect. Collectively, these results imply that both SOS2L and GmbZIP131 are capable of positively modulating the expression of the *GmICHG* gene, which in turn appears to play a pivotal role in the soybean's adaptive response to saline conditions (Supplementary Fig. S11C). As SOS2 and its homologs play crucial roles in mediating plant salt responses, the interaction between GmbZIP131 and GmSOS2L may allow them to cooperatively regulate salinity responses.

Given that GmSOS2L is a protein kinase, we verified whether it could phosphorylate GmbZIP131. An in vitro kinase assay with recombinant His-GmSOS2L and His-GmbZIP131 proteins proves that GmSOS2L could phosphorylate GmbZIP131 in the presence of ATP (Fig. 7A). Given the possibility of nonspecific binding with the antithiophosphate ester rabbit antibody as noted by Jiang et al. (2023), we conducted MS analysis on the tryptic peptides of His-GmbZIP131 (Fig. 7B). This analysis targeted the product of the aforementioned in vitro phosphorylation reaction to accurately pinpoint the phosphorylation sites. MS results indicate that, in the in vitro kinase reaction system, GmSOS2L phosphorylates GmbZIP131 exclusively at the S135 residue. To validate this finding, we expressed both GmbZIP131-S135A and GmbZIP131-S135D proteins in *Escherichia coli*, alongside the WT GmbZIP131 protein, and performed the in vitro kinase reaction again. The results showed that when the S135 residue was mutated to either A or D, no phosphorylation signal of GmSOS2L on GmbZIP131 was detected (Supplementary Fig. S12). These findings suggest that S135 is the sole phosphorylation site for GmSOS2L on GmbZIP131.

To ascertain the presence of the S135 phosphorylation on the GmbZIP131 in vivo, we assessed the protein phosphorylation

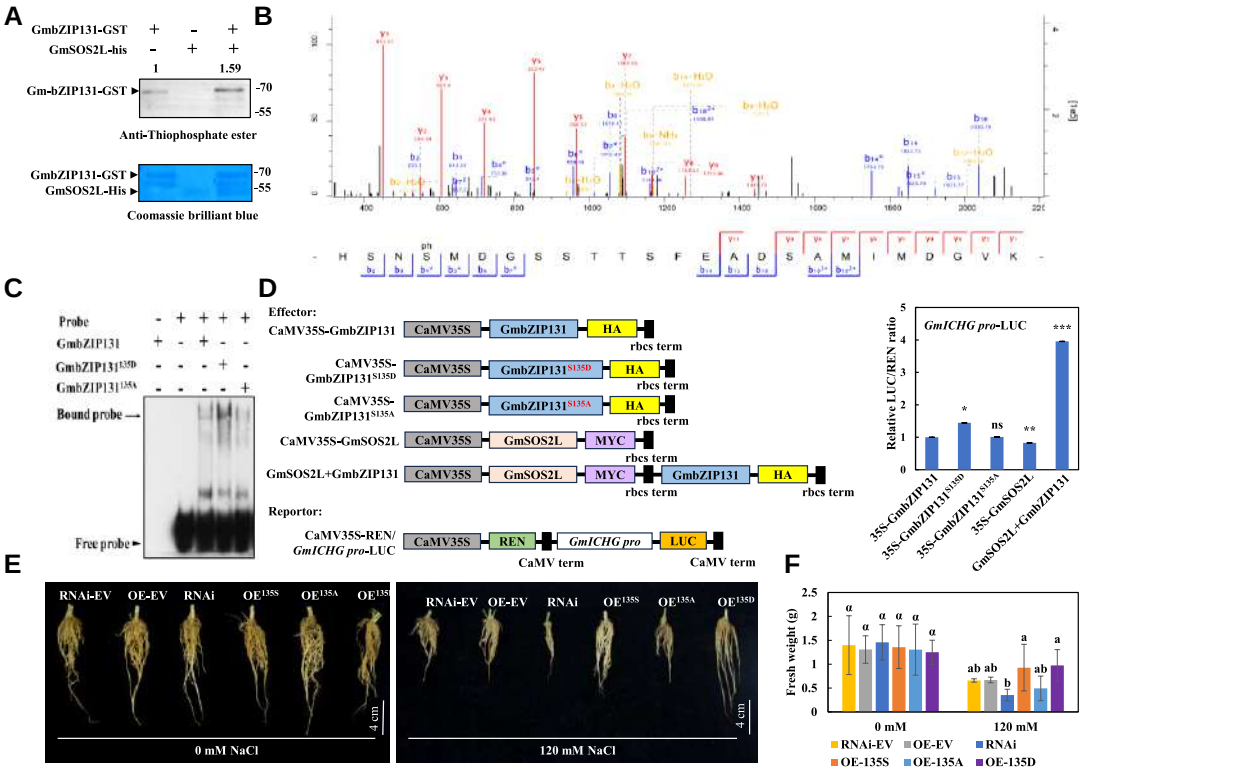

Figure 7. GmbZIP131 enhances salt tolerance via GmSOS2L-dependent phosphorylation. **A)** GmSOS2L phosphorylates GmbZIP131 in vitro. Recombinant GmbZIP131-GST, when phosphorylated, was detected using antithiophosphate ester rabbit monoclonal antibodies following SDS–PAGE (top panel), with Coomassie brilliant blue staining serving as a loading control (bottom panel). **B)** Mass spectrometric identification of the in vitro phosphorylation site Ser135 on GmbZIP131 peptide fragments by GmSOS2L. The x-axis denotes the mass-to-charge ratio (m/z), measured in Daltons per charge (Da/e). The left y-axis reflects the relative abundance of ions, whereas the right y-axis corresponds to the signal intensity of the detected ions. **C)** EMSA using biotin-labeled probes of GmICHG containing WT G-box elements incubated with GmbZIP131, GmbZIP131^{135D}, and GmbZIP131^{135A} mutants. The arrow indicates the position of the specifically bound probe. Samples were resolved on a 6% polyacrylamide gel. **D)** DLR assays confirm the enhancement of GmbZIP131 transactivation activity by GmSOS2L-induced phosphorylation on the GmICHG promoter. Statistically significant differences ($P < 0.05$) were analyzed using Student's t-test. **E** and **F)** Phenotypic characterization of soybean hairy roots transformed with RNAi-EV (*pTCK303-DsRed* EV), OE-EV (*pDL28-DsRed* EV), RNAi (*pTCK303-GmbZIP131-DsRed*), and 135S/A/D-OE (*pDL28-GmbZIP131*$^{S135S/A/D}$*-DsRed*). RNAi-EV and OE-EV served as control groups. The soybeans were exposed to a 7 d treatment with 120 mM NaCl, with 1/4-strength Hoagland's solution used as the control. Data in **D** and **F** are presented as mean ± SD from at least 3 independent biological replicates for each genotype and treatment condition. Different letters indicate statistically significant differences at $P < 0.05$ by 1-way ANOVA followed by Duncan's significant difference test. The experiments presented in **A**, **C**, and **E** were repeated 3 times with consistent results. **E** and **F)** The labels "0 mM" and "200 mM" on the x-axis represent the concentrations of the salt treatment.

profiles of soybean roots subjected to salt stress versus control conditions. Our findings indicate that the phosphorylation at S135 on the GmbZIP131 is enhanced under salt stress (Supplementary Table S11). This elevation in S135 phosphorylation is in alignment with the in vitro kinase assay results, which demonstrated that GmSOS2L mediates the phosphorylation of GmbZIP131 at this residue. Collectively, these observations suggest a convergence between the in vitro phosphorylation events and the in vivo phosphoproteomic triggered by salt stress, highlighting a specific regulatory mechanism within the soybean stress response network.

GmbZIP131 confers salt tolerance in a phosphorylation manner

We further explored the influence of GmSOS2L-induced phosphorylation on the interaction between GmbZIP131 and the *GmICHG* promoter, as well as its subsequent impact on transcriptional expression. EMSAs revealed that the phosphor-mimic GmbZIP131^{135D} mutant protein exhibited notably higher binding affinity for the *GmICHG* promoter compared with the WT GmbZIP131 protein, whereas the phosphor-ablative GmbZIP131^{135A} mutant displayed minimal binding affinity (Fig. 7C). These findings suggest that phosphorylation at the S135 residue might enhance the binding affinity of GmbZIP131 to the *GmICHG* promoter.

Subsequently, we evaluated the promoter activity of *GmICHG* using a DLR assay by introducing *GmbZIP131*, *GmbZIP131*^{135D}, *GmbZIP131*^{135A}, or a combination of *GmbZIP131 and GmSOS2L*, into *N. benthamiana* leaves. The activity of the *ProGmICHG::LUC* reporter exhibited a significant increase upon co-transformation with both GmbZIP131 and GmSOS2L, contrasting with the activity levels observed when GmbZIP131 was co-transformed in isolation (Fig. 7D). Consistent with the abovementioned beneficial effect of GmSOS2L-induced phosphorylation, GmbZIP131^{135D} displayed enhanced transactivation of the *ProGmICHG::LUC* reporter compared with both the WT GmbZIP131 and the GmbZIP131^{135A} mutant (Fig. 7D). These results indicate that the augmented transactivity of GmbZIP131 is dependent on phosphorylation at Ser135 mediated by GmSOS2L.

In summary, our findings clarify that GmSOS2L-induced phosphorylation at S135 augments GmbZIP131's binding affinity to the

CACGTG *cis*-element within the *GmICHG* promoter, thereby enhancing its transcriptional activity.

To ascertain the regulatory role of S135 phosphorylation on GmbZIP131's biological functions concerning soybean's salinity tolerance, we developed transgenic soybean hairy roots with enhanced expression of *GmbZIP131* (OE^{135S}), *GmbZIP131*^{S135A} (OE^{135A}), and *GmbZIP131*^{S135D} (OE^{135D}), as well as those with *GmbZIP131-RNAi* knockdown. The empty OE (OE-EV) and RNAi vectors (RNAi-EV) served as negative controls. Soybeans were transformed using *Agrobacterium rhizogenes* harboring vectors for either GmbZIP131$^{S135S/A/D}$ OE or GmbZIP131 knockdown. Given the presence of an autonomous 35S::*DsRed* expression cassette in each vector, transgenic hairy roots were identified through red fluorescence (Supplementary Fig. S13). Plants with red fluorescent hairy roots were treated hydroponically with 120 mM NaCl.

The results indicated that the 6 transgenic soybean lines did not exhibit significant phenotypic differences under control conditions. Upon salt treatment, the hairy roots transformed with RNAi-EV and OE-EV grew similarly, suggesting that transformation with the EVs did not affect soybean growth, thus validating their use as controls. In contrast to the EVs, the GmbZIP131-RNAi roots showed the most pronounced damage, indicating that silencing GmbZIP131 significantly compromised salt resistance. Among the transformed roots, those with the OE^{135D} construct exhibited the least salt inhibition, followed by OE^{135S} and then OE^{135A}, indicating that the phosphor-mimetic GmbZIP131 at Ser135 enhances soybean's salinity tolerance (Fig. 7, E and F). Collectively, these findings imply that GmbZIP131 modulates soybean's salt tolerance in a manner dependent on Ser135 phosphorylation.

Additionally, we aimed to further investigate whether SOS2L and GmICHG can regulate the accumulation of flavonoid compounds. To explore this, we generated transgenic roots overexpressing *GmSOS2L* (SOS2L-OE) and *GmICHG* (GmICHG-OE) using hairy root transformation, with an EV as the control. We then analyzed the metabolites, focusing on isoflavone and flavonoid compounds, in these transgenic roots following treatment with 120 mM NaCl. The results revealed that, after excluding redundant metabolites, a total of 1,886 metabolites were detected in both negative and positive ionization modes (Supplementary Figs. S14 to S16 and Table S12). Of these, 372 metabolites were upregulated by GmSOS2L and 375 by GmICHG under control conditions, while 366 metabolites were upregulated by GmSOS2L and 214 by GmICHG under salt treatment (Supplementary Fig. S14). Notably, 53 metabolites involved in isoflavone biosynthesis (Fig. 8 and Supplementary Table S14) and 201 metabolites linked to flavonoid biosynthesis exhibited differential accumulation (Supplementary Table S15). Interestingly, both lupiwighteone and lupiwighteone 7-glucoside were positively regulated by GmSOS2L and GmICHG (Fig. 8). These findings, which align with the metabolic data regulated by GmbZIP131 (Fig. 5), suggest that these metabolites play crucial roles in the plant's response to salt stress and are likely synergistically regulated by proteins such as SOS2L, GmbZIP131, and GmICHG.

Discussion

The plant's response to high salinity is governed by a complex array of molecular mechanisms (Munns and Tester 2008). Prominent among these is the SOS pathway, pivotal for preserving ion homeostasis during salt stress (Zhu 2016). However, the current understanding of SOS2 primarily focuses on its involvement in excluding Na^+ ions, with limited attention given to other signaling pathways. Some evidence suggests that the SOS pathway is also involved in the regulation of ROS within plants, which is extremely important for plants to withstand the detrimental effects of salt stress. The SOS pathway in plants is a well-known regulatory factor in salt tolerance, playing a key role in the removal of excessive ROS induced by salt stress. Our previous studies have also highlighted the important role of flavonoids in clearing excessive ROS under salt stress (Pi et al. 2018, 2019). Given that the SOS pathway functions at an early stage of the salt tolerance response, while flavonoids act at a later stage, both play critical roles in regulating ROS clearance and maintaining ROS balance under salt stress. We therefore hypothesize that there may be indirect connections between the SOS signaling pathway and the action of flavonoids. As key regulators of both flavonoid biosynthesis and ROS modulation, bZIP transcription factors could serve as a bridge linking the SOS pathway with flavonoid function.

Verslues et al. (2007) provided insights into the critical role of SOS2 in maintaining H_2O_2 homeostasis under salt stress, highlighting its interactions with NDPK2, CAT2, and CAT3. SOS2 links H_2O_2 metabolism and signaling through these interactions, underscoring its multifaceted involvement in the plant's response to salt stress. SOS1, functioning as a plasma membrane Na^+/H^+ antiporter, engages with RCD1, a protein implicated in oxidative stress tolerance, via its predicted C-terminal cytoplasmic tail (Katiyar-Agarwal et al. 2006). This interaction not only reveals a function of SOS1 in oxidative stress tolerance but also connects ion homeostasis with oxidative stress detoxification pathways, both of which are integral to plant salt stress endurance. ENH1 contributes to plant salt tolerance by participating in the detoxification of ROS induced by salt stress. Zhu et al. (2007) suggested that ENH1 might be involved in ROS detoxification through a salt tolerance pathway that potentially includes the SOS2 signaling component. These findings underscore the diverse roles of the SOS pathway in ion homeostasis and ROS regulation, further confirming its significance in plant adaptation to salt stress.

In soybean, the SOS2 putative ortholog, GmSOS2L, alternatively named GmPKS4, functions as a protein kinase that is distributed across both the nucleus and cytoplasm. This kinase has been associated with bolstering the plant's salinity tolerance, where it plays a role in the neutralization of ROS and in reinforcing the transcriptional regulation of stress-responsive genes (Ketehouli et al. 2021). Our study corroborates the findings reported by Ketehouli et al. (2021), demonstrating that the OE of *GmSOS2L* significantly ameliorates the salt tolerance of soybean. This enhancement is hypothesized to stem from the activation of the GmbZIP131 transcription factor, which in turn stimulates the transcriptional expression of the *GmICHG* gene. The upregulation of *GmICHG* is posited to govern flavonoid synthesis, thereby contributing to ROS scavenging. This discovery establishes a link between the SOS pathway and flavonoid-mediated response to oxidative stress induced by salt stress, highlighting a complex network of signaling and defense mechanisms in plants.

GmbZIP131 is a bZIP transcription factor in soybean, classified within Subfamily I as depicted in Supplementary Fig. S1. Members of this subfamily are recognized for their pivotal roles as regulatory modulators in orchestrating the plant's adaptive responses to a multitude of environmental stressors (Yu et al. 2020). Our investigation has uncovered that GmbZIP131 undergoes phosphorylation at serine 135 by the kinase GmSOS2L, a critical posttranslational modification that is specifically induced by salt stress. Phosphorylation of GmbZIP131 at S135 by GmSOS2L increases its affinity for binding to the *GmICHG* promoter. This enhanced binding capacity promotes the accumulation of

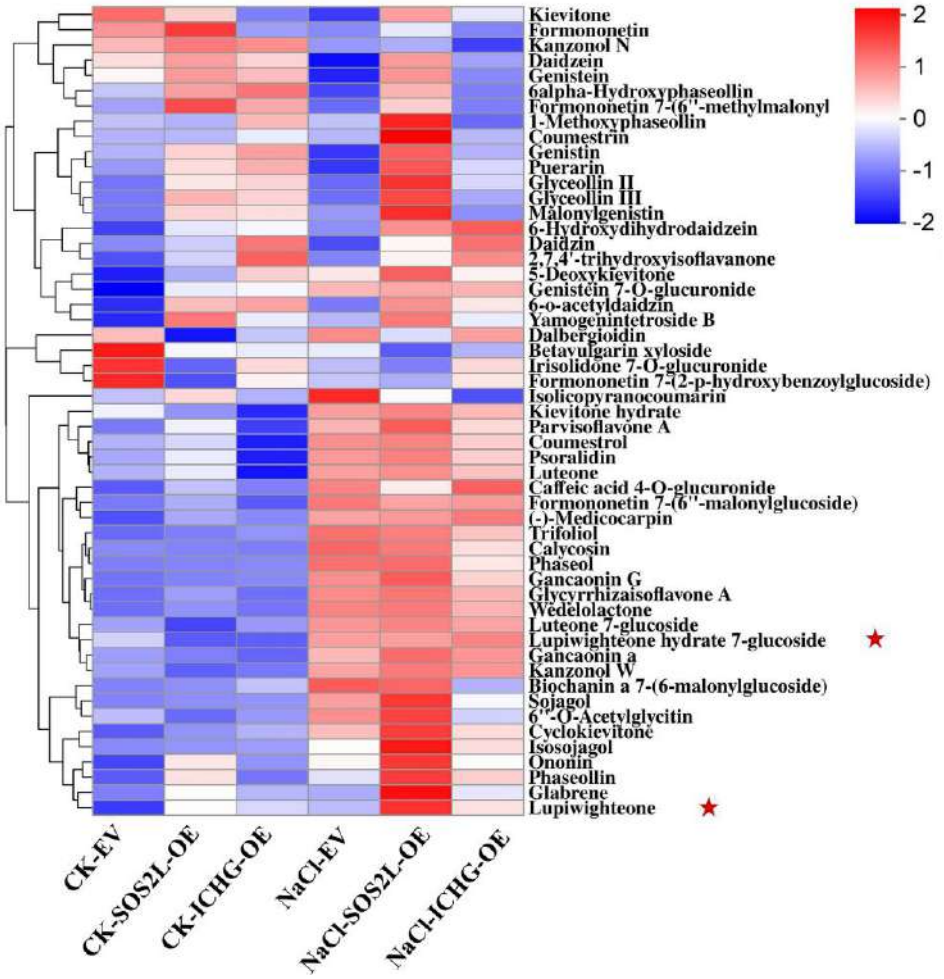

Figure 8. GmSOS2L and GmICHG positively regulate the accumulation of isoflavones, particularly lupiwighteone and lupiwighteone 7-glucoside. Differentially accumulated isoflavones were analyzed in soybean hairy roots transformed with the EV, P_{35S}::*GmSOS2L* (SOS2L-OE), and P_{35S}::*GmICHG* (ICHG-OE) under both control and 120 mM NaCl conditions. The results were visualized in a heat map. The metabolites lupiwighteone and lupiwighteone 7-glucoside are highlighted by 2 pentagram symbols. The color scale bar indicates relative abundance levels of isoflavones.

flavonoids and improves the plant's ability to neutralize peroxides, thereby significantly enhancing soybean salt tolerance.

The generation of ROS in different subcellular compartments is a characteristic response of plants to various stress factors. ROS signaling plays a crucial role in connecting events that take place in key subcellular locations, particularly the apoplast, chloroplast, and nucleus (Shapiguzov et al. 2012). Consequently, the apoplast serves as a major site for the generation and accumulation of ROS in plants following stress. Maintaining a balance of ROS levels in the apoplast is an important mechanism for plants to withstand stress. Flavonoids, acting as essential antioxidants and signaling molecules, are involved in various stress responses (Ferreyra et al. 2012). The biosynthesis of flavonoids is often induced by abiotic stresses and tightly regulated by a diverse array of transcription factors (Hassani et al. 2020). In our study, we have demonstrated that GmbZIP131 upregulates the expression of *GmICHG*, leading to an increase in isoflavone production. GmICHG is a beta-glucosidase enzyme that is localized in the apoplast and specifically hydrolyzes the beta-7-O-(malonyl) glucosides of isoflavones, resulting in the formation of free isoflavones with enhanced biological activity and bioavailability (Kumar et al. 2023). Therefore, the expression of *GmICHG* is crucial for the synthesis of biologically active isoflavones. Indeed, our findings demonstrate that the OE of *GmICHG* significantly improves the salt tolerance of transgenic soybean hairy roots. This leads us to hypothesize that the free isoflavones generated through the enzymatic action of GmICHG on isoflavone-beta-7-O-(malonyl) glucoside precursors could be instrumental in the soybean's response to salt stress. The proposed function of these free isoflavones is likely centered on their capacity to neutralize peroxides.

However, mechanisms by which beta-7-O-(malonyl) glucosides of isoflavones are transported from within the cell, particularly from the vacuolar compartment, to the apoplast in counteracting excessive ROS accumulation under conditions of salt stress remain an open question. Several ATP-binding cassette (ABC) transporters have been found to facilitate the transport of isoflavone glycosides from vacuoles to the apoplast (Gani et al. 2021), and this transport capacity may be enhanced after exposure to salt stress. Previous studies have shown that salt stress can lead to an alkalinization of vacuoles, resulting in a pH shift to ~7.82 (Kader and Lindberg 2010; Shen and Zhao 2023). The transport activity of ABC transporters increases with an elevated pH, ranging from 6.0 to 8.0 (Sugiyama et al. 2007), suggesting that salt stress can raise the pH of vacuoles and consequently enhance the outward transport of isoflavone glycosides mediated by ABC transporters.

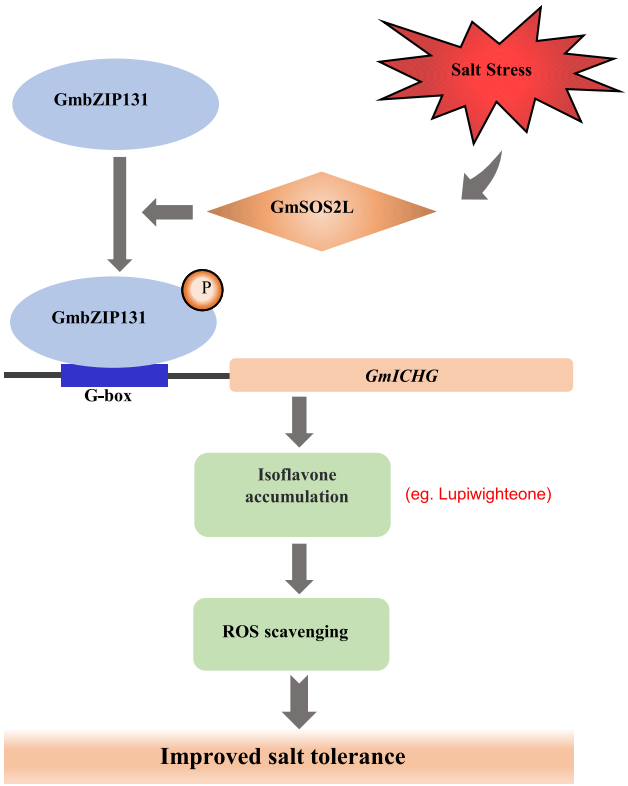

Figure 9. Proposed model depicting the intricate regulatory network of GmbZIP131 in response to salt stress. Upon exposure to salt stress, SOS2 is activated and phosphorylates GmbZIP131. Activated by this phosphorylation event, GmbZIP131 upregulates its target gene *GmICHG*, which encodes an enzyme that hydrolyzes lupiwighteone 7-glucoside, resulting in the release of lupiwighteone in the apoplast. Subsequently, lupiwighteone acts as a scavenger for excess ROS, thereby mitigating the oxidative stress induced by salt.

In summary, our research introduces an integrative model that delineates the molecular underpinnings of the salt stress response mechanism in soybean, with a particular emphasis on the pivotal role of GmbZIP131 (Fig. 9). Upon encountering salt stress, the activation of the protein kinase SOS2 initiates a phosphorylation cascade that targets GmbZIP131. This transcription factor is instrumental in modulating the expression of its downstream gene, *GmICHG*. This gene encodes an enzyme that catalyzes the conversion of lupiwighteone 7-glucoside to the more biologically active lupiwighteone in the apoplast. Notably, lupiwighteone functions as an efficacious antioxidant, capable of scavenging ROS (Erasto et al. 2004; Ren et al. 2015), thus alleviating the oxidative stress associated with salt exposure. Consequently, our study underscores the critical role of GmbZIP131 in facilitating the interplay between the SOS pathway and flavonoid biosynthesis, which collectively contribute to the modulation of soybean's salt tolerance.

Materials and methods

Plant materials and cultivation conditions

Seeds of WT soybean (Tianlong 1#), *GmbZIP131*-overexpressing (GmbZIP131-OE), and *GmbZIP131* knockdown (RNAi) transgenic lines were sown in a sterilized 1:1 (v/v) mixture of nutrient-rich soil and perlite. Plants were cultivated in a controlled growth chamber under a 12 h light/12 h dark photoperiod at 28 °C and 60% relative humidity, with illumination of 200 μmol/m^2 s.

The seeds of *N. benthamiana* were sown in a 1:1 (v/v) mixture of nutrient-rich soil and vermiculite. Four-week-old *N. benthamiana* plants were employed for subcellular localization assay, LCI, BiFC, and DLR analyses. They were grown under a 14 h light/10 h dark photoperiod at 25 °C and 60% relative humidity, with illumination of 100 μmol/m^2 s.

RNA extraction and RT-qPCR

Total RNA from samples was extracted using the RNAiso Plus (catalog no. 9109; TaKaRa, Kyoto, Japan), according to the manufacturer's instructions. One microgram of total RNA was reverse transcribed into cDNA using the HiScript II 1st Strand cDNA Synthesis Kit (catalog no. R211-01; Vazyme, Nanjing, China). The resultant cDNA was diluted to 200 ng/μL with RNase-free water. RT-qPCR was performed using the AceQ qPCR SYBR Green Master Mix (Without ROX) (catalog no. Q121-02; Vazyme), following the manufacturer's protocol. The relative expression levels were calculated using the $2^{-\Delta\Delta Ct}$ method (Livak and Schmittgen 2001) with *GmActin11* as the internal control. *GmActin11* is a housekeeping gene commonly used as an internal control in RT-qPCR analyses and demonstrates stable expression under different conditions (Ma et al. 2013; Gao et al. 2021; Ketehouli et al. 2021; Zhang et al. 2024). Three biological replicates for each sample and 3 technical replicates for each biological replicate were conducted. All primers used in this research are listed in Supplementary Table S13.

Generation of transgenic soybean and salt treatment

To generate *GmbZIP131*-overexpressing transgenic soybean, the full-length coding sequence (CDS) of *GmbZIP131* was amplified and cloned into the plant expression vector *pDL28* (a derivative of pCAMBIA1300 incorporated with a P_{35S}::*Bar* expression cassette) by *KpnI* site under the control of the cauliflower mosaic virus 35S promoter. To generate *GmbZIP131* knockdown transgenic soybean, a 484 bp fragment of the *GmbZIP131* CDS was amplified and inserted into the RNAi vector pTCK303 in sense and antisense orientations. The phosphinothricin acetyltransferase gene was also introduced into both constructs as a plant selection marker. The resultant plasmids were transformed into *Agrobacterium tumefaciens* strain EHA105, which was used to generate transgenic soybean through cotyledon transformation (Wang et al. 2021). Leaves from 14-d-old transgenic seedlings were collected for genomic DNA and total RNA extraction, followed by PCR analysis.

Seven-day-old seedlings with uniform growth were transferred into 36-well boxes containing modified 1/4 Hoagland's solution. After the emergence of the first trifoliate leaves, 200 mM NaCl was added. As control, 1/4 Hoagland's solution was used. The seedlings were cultured for another 24 h before sample collection. After treatment, samples including roots, stems, and leaves were collected immediately and frozen in liquid nitrogen for further use.

Soybean hairy root transformation and phenotyping after salt treatment

For the induction of hairy roots as described by Kereszt et al. (2007) for salt stress analysis, 5-d-old soybean (Tianlong 1#) seedlings were subjected to transformation with *Ag. rhizogenes* strain K599 harboring *pTCK303-DsRed*, *pTCK303-GmbZIP131-DsRed*, *pDL28-DsRed*, *pDL28-GmbZIP131*$^{S135S/A/D}$*-DsRed*, *pDL28-GmICHG-DsRed*, and *pDL28-GmSOS2L-DsRed*, respectively. Once the hairy root was 3 to 5 cm in length, the primary root was excised.

Transgenic hairy roots that exhibited DsRed fluorescence were identified using a Zoom Stereo microscope (SMZ1270; Nikon), with nonfluorescent roots being eliminated. The ensuing "composite" soybean plants were subjected to a 7 d treatment with 120 mM NaCl to ascertain the fresh weight of the introduced genetic modifications under saline stress conditions. Roots were frozen in liquid nitrogen and stored at −80 °C for subsequent gene-expression analysis. All experiments were performed with a minimum of 3 repetitions.

Physiological analysis and histochemical staining

Root, stem, and leaf tissues from both control and NaCl-treated samples were analyzed to quantify MDA levels (Yan et al. 2014) and assess POD activity (Wang et al. 2010). The concentrations of H_2O_2 were determined using the respective detection kits (catalog no. C500060-0250; Sangon Biotech, Shanghai, China), strictly following the provided user manuals. The in situ accumulation of H_2O_2 and O_2^- within the leaves was visualized through histochemical staining with DAB and NBT, respectively, as per the method described by Huang et al. (2013).

Flavonoid content

The quantification of total flavonoid content was performed in accordance with a previously established method (Dash et al. 2017). To assess flavonoid levels, root tissues were harvested from specimens grown under normal and NaCl stress conditions. Flavonoid quantification was performed using the aluminum chloride colorimetric assay. Briefly, 0.1 g of root extract was mixed with 1 mL of 80% methanol and incubated at 50 °C for 2 h. Then, 0.5 mL of the mixture was combined with 4.5 mL of 2% $AlCl_3$ solution and incubated at room temperature for 30 min. A calibration curve was established using rutin dissolved in 80% methanol, with concentrations ranging from 2 to 100 μg/mL. Absorbance at 415 nm was measured, and flavonoid content was expressed as rutin equivalents in milligrams per gram of tissue.

RNA-seq analysis of transgenic soybean

Total RNA was isolated in triplicate from the roots of GmbZIP131-OE, GmbZIP131-RNAi seedlings treated with 200 mM NaCl or 0 mM NaCl (as control) for 24 h. While the seedling was collected, it was immediately frozen in liquid nitrogen and stored at −80 °C. Total mRNA was isolated using the MJZol total RNA extraction kit (Majorbio Bio-Pharm Technology, Shanghai, China), quality checked on Agilent 2100 Bioanalyzer, quantified using the ND-2000 (NanoDrop Technologies), and used for RNA-seq library construction with the Illumina Truseq RNA sample prep Kit (Illumina, San Diego, CA, USA), according to the manufacturer's instructions. The paired-end reads were obtained and sequenced (paired-end, 150 bp each) with the NovaSeq 6000 sequencer. After removing adaptor and low-quality reads, clean reads were mapped to *G. max* (assembly Glycine_max_v4.0) using HISAT2 (Kim et al. 2015) and assembled using Cufflinks (Trapnell et al. 2010). Differential expression analysis was conducted on 2 samples using the DESeq2 algorithm. Genes with a false discovery rate (FDR) ≤ 0.05 were considered to be significantly differentially expressed. In addition, functional-enrichment analysis KEGG was performed to identify which differentially expressed genes (DEGs) were significantly enriched in metabolic pathways at Bonferroni-corrected *P*-value ≤0.05 compared with the whole-transcriptome background. KEGG pathway analysis was carried out by KOBAS (Mao et al. 2005).

Subcellular localization analysis

The full-length *GmbZIP131* CDS, lacking the stop codon, was amplified and cloned into the *pCAMBIA1300-35S::GFP* vector to generate the *35S::GmbZIP131-GFP* construct, while the *35S::GFP* construct served as a control. To investigate the subcellular localization of GmbZIP131, vectors expressing *GFP* fused to the full-length *GmbZIP131* cDNA were generated and co-expressed with the nuclear marker D53-mCherry (Zhou et al. 2013) in 4-wk-old *N. benthamiana* leaves (Chen et al. 2008). The fluorescence signals of GFP were then observed using a confocal laser scanning microscope (LSM900). GFP (laser intensity: 4.5% to 7.5%, excitation wavelength: 493 nm, emission wavelength: 482 to 570 nm, gain: 622 V); mCherry (laser intensity: 0.7% to 0.8%, excitation wavelength: 577 nm, emission wavelength: 560 to 626 nm, gain, 641 V).

Fractionation experiments were also performed to confirm the distribution of the GmbZIP131 protein in the nucleus. Cytosolic (C) and nuclear (N) proteins were extracted from *N. benthamiana* leaves transformed with P_{35S}::*GmbZIP131-HA* or an EV, and then analyzed by immunoblotting using the indicated antibodies. Anti-Rubisco (M20044M; Abmart, Shanghai, China) and antihistone H3 (P30266M; Abmart) antibodies were used as markers for the cytosolic and nuclear fractions, respectively.

ChIP–PCR assay

The full-length CDS of *GmbZIP131* was subcloned into the *pDL28-HA/Ubq10::DsRed* vector, forming *pDL28-35S::GmbZIP131-HA/Ubq10:: DsRed*, and the EV was used as a negative control. Then, the 2 constructs were transformed into the WT soybean via *Ag. rhizogenes* strain K599. The composite plants with transgenic roots were treated with 120 mM of NaCl in 1/4-fold Hoagland's solution for 7 d and the transgenic roots were verified by their expression of *DsRed*. Subsequently, the tissues were fixed with a 1% (v/v) formaldehyde crosslinking method for 15 min. ChIP–PCR assays were performed, as previously described (Pi et al. 2019). Immunoprecipitation reactions were performed using an anti-HA antibody (catalog no. sc-7392; Santa Cruz) and chromatin prior to immunoprecipitation (IP) was used as an input control. Complexes of chromatin antibodies were captured with protein G beads. Enriched DNA fragments were identified by PCR analysis.

Electrophoretic mobility shift assays

The full-length CDSs of *GmbZIP131* and mutants were cloned into the *pET28a* vectors to generate *His-GmbZIP131*^{WT,A,D} constructs. His-GmbZIP131 recombinant protein was expressed in *E. coli* strain BL21 (DE3) pLysS and purified with Ni-NTA Sefinose (TM) Resin 6FF (Settled Resin) (catalog no. C600033-0100; Sangon Biotech). The purified fusion protein and biotin-labeled DNA probes containing G-box *cis*-elements were used for EMSAs. EMSAs were carried out using the Light Shift Chemiluminescent EMSA Kit (catalog no. GS009; Beyotime Biotech, Shanghai, China), according to the manufacturer's instructions.

DLR assays

The DLR assay was executed in accordance with the methodology reported by Li et al. (2020). In this assay, the 2.0 kb promoter region upstream of *GmICHG* was cloned and embedded into the pGreen II 0800-LUC vector, employing the primers specified in Supplementary Table S13. The resultant recombinant plasmids were subsequently transformed into the Agrobacterium strain GV3101 (pSoup-p19) (catalog no. CC96303; Tolo Biotech, Shanghai, China). The GmbZIP131 protein was mixed with the promoter

sequences at a volume ratio of 1:9 and injected into young *N. benthamiana* leaves to facilitate transient co-transformation and expression analysis. The comparative transactivation activities of firefly and renilla luciferase were measured using the Dual-Luciferase Reporter Gene Assay Kit (catalog no. RG027, Beyotime Biotech), strictly following the manufacturer's protocol.

Y2H assays

A cDNA library of WT soybean seedlings was created using the Matchmaker GAL4 Two-Hybrid System 3 following the instructions (protocol no. PT3247-1; Clontech). For Y2H assays, the CDSs of *GmbZIP131* and *GmSOS2L* were cloned into the *pGBKT7* and *pGADT7* vectors, respectively, and the recombinant plasmids were then co-transformed into the yeast strain AH109. The Y2H assays were carried out as per the manufacturer's guidelines.

LCI assays

LCI assays were conducted following the previously described methods (Chen et al. 2008). The CDSs of *GmSOS2L* and *GmbZIP131* were cloned into the *pCAMBIA1300-cLUC* and *pCAMBIA1300-nLUC* vectors, respectively. Afterward, *Ag. tumefaciens* strain GV3101 (catalog no. TSC-A01; Tsingke Biotechnology, Beijing, China) carrying different plasmids was mixed to a final concentration of $OD_{600} = 1$ and incubated at room temperature for 2 h. Four different combinations of Agrobacterium were injected into 4 different positions in the same leaves of *N. benthamiana* and cultured for 48 h. Seven minutes before detection, 0.2 mM D-luciferin (catalog no. 40903ES01; Yeasen, Shanghai, China) was evenly applied to the same positions into which Agrobacterium was injected. A low-light cooled charge-coupled device imaging device (CA2048B Lumazone) was used to capture the LUC signal. At least 6 independent leaves were used for each experiment, and 3 biological replicates were performed with similar results.

BiFC assays

To conduct BiFC assays, we cloned the full-length CDSs of *GmSOS2L* and *GmbZIP131* without stop codon into the *pDOE-03* vector, resulting in the generation of *pDOE03-35S:GmbZIP131-NmVen210-35S:GmSOS2L-CVen210* recombinant reporter fusion construct, which was then transformed into *Ag. tumefaciens* strain GV3101 and infiltrated into *N. benthamiana* leaves. Subsequent experimental methodologies were similar to LCI assays. The Venus and DAPI signals were observed with a confocal laser scanning microscope (LSM710; Zeiss) YFP (laser intensity: 2.0% to 3.3%, excitation wavelength: 488 nm, emission wavelength: 493 to 630 nm). DAPI (laser intensity: 2.0% to 3.3%, excitation wavelength: 405 nm, emission wavelength: 410 to 585 nm).

Pull-down assay

A pull-down assay was conducted in accordance with the methodology detailed by Ren et al. (2021), utilizing glutathione magarose beads following the guidelines provided by the manufacturer (SM002100; Smart-Lifesciences, Changzhou, China). The complete cDNA sequence of GmbZIP131 was inserted into the *Xho*I restriction site of the pGEX-6P-1 vector to produce the recombinant protein GST-GmbZIP131. Similarly, GmSOS2L was integrated into the *Sac*I and *Xho*I sites of the pET28a vector, yielding the fusion protein His-GmSOS2L (with primer sequences delineated in Supplementary Table S13). The expression of the GST-GmbZIP131 and His-GmSOS2L fusion proteins was achieved in *E. coli* BL21 (DE3) (C504-02; Vazyme) and Arctic-Express (DE3) (catalog no. 230192; SH Biotech, Shanghai, China) strains, respectively, through induction with 0.2 mM isopropyl β-D-thiogalactoside.

Subsequently, the GST-GmbZIP131 fusion protein, or the GST-Tag was immobilized onto glutathione magarose beads and then incubated with extracts containing His-GmSOS2L or His-tag. Following a 4 h incubation at 4 °C on a rotary shaker, the beads were thoroughly washed 5 times with ice-cold phosphate-buffered saline, resuspended in SDS–PAGE loading buffer, and subsequently applied to SDS–PAGE gels.

For western blot detection, primary antibodies specific for anti-GST (catalog no. D110271-0100; Sangon Biotech) or anti-His (catalog no. D110002-0100; Sangon Biotech) were applied at a dilution of 1:5,000. The secondary antibody used was antirabbit, diluted to 1:5,000 (catalog no. BK-R050; Bioker Biotech, Hangzhou, China). The western blots were visualized using an enhanced chemiluminescence detection reagent (catalog no. 4AW012-500; 4A Biotech, Beijing, China).

In vitro phosphorylation assay and alkylation

In vitro phosphorylation assays were executed in accordance with the methods outlined by Jiang et al. (2023). Recombinant GST-GmbZIP131 (1,000 ng) was mixed with the substrate proteins maltose binding protein His-GmSOS2L (100 ng) within a kinase reaction buffer composed of 20 mM HEPES at pH 7.4, 150 mM NaCl, 10 mM $MgCl_2$, and 1 mM ATPγS (catalog no. ab138911; Abcam, Cambridge, United Kingdom). This mixture was incubated at 30 °C for a duration of 1 h. Subsequently, 1.5 μL of 50 mM PNBM (catalog no. ab138910; Abcam) was introduced to the reaction mixture, which was further incubated at 30 °C for 1.5 h. Recombinant proteins were separated through 10% (w/v) SDS–PAGE, and the phosphorylated GST-GmbZIP131 was detected via immunoblotting utilizing a diluted antithiophosphate ester antibody at a ratio of 1:5,000 (catalog no. ab92570; Abcam).

In vitro kinase activity and LC–MS/MS analysis

The CDS of *GmSOS2L* was inserted into *pET28a* and transformed into *E. coli* strain BL21 (DE3) pLysS to express recombinant *His-GmSOS2L*. The purified His-GmSOS2L and His-GmbZIP131 were used to test whether GmbZIP131 could be phosphorylated by GmSOS2L. The substrate phosphorylation assay was performed, as described previously (Pi et al. 2018). Briefly, the GmSOS2L and GmbZIP131 were added into the kinase buffer containing HEPES (20 mM, pH 7.4), $MgCl_2$ (10 mM), NaCl (150 mM), 50 μM ATP, and reacted for 30 min at 25 °C. Finally, the reaction was stopped with SDS loading buffer and electrophoresed on a 10% SDS–PAGE for further LC–MS/MS analysis.

LC–MS/MS analysis was performed by the Micrometer Biotech Company (Hangzhou, China). Briefly, the peptide fragments formed after trypsin cleavage were separated by LC and ionized by a nano-ESI source and then passed to a Thermo Fisher LTQ Obitrap ETD (Thermo Fisher Scientific, San Jose, CA, United States) for data-dependent acquisition mode detection. The raw LC–MS/MS data were processed using Proteome Discoverer 1.4 (Thermo). The main parameters were set as follows: maximum missed cleavage site, 2; minimum peptide length, 6 amino acids; precursor mass tolerance, 20 ppm; fragment mass tolerance, 0.05 Da; static modifications, carbamidomethylation (Cys), oxidation (Met), and acetylation on protein N-terminus; maximum variable posttranslational modifications per peptide, 3; and FDR for protein, peptide, and modification site, 1%. Differential expression analysis of proteins was conducted using the

Student's *t*-test, with a significance threshold set at $P < 0.05$. Subsequently, KEGG pathway analysis was performed using KOBAS (Mao et al. 2005).

Nontargeted LC–MS–based metabolomics analysis

Roots were collected from the 2-wk-old *GmbZIP131*-OE, *GmbZIP131*-RNAi, and WT plants treated with 0 and 200 mM NaCl for 24 h (with 3 replicates per sample) for metabolome analysis, performed by Micrometer Biotech Company. The collected samples were thawed on ice, and metabolites were extracted with 80% methanol buffer. Briefly, 50 mg of sample was extracted with 0.5 mL of precooled 80% methanol. The extraction mixture was then stored for 30 min at −20 °C. After centrifugation at 20,000×*g* for 15 min, the supernatants were transferred into a new tube and vacuum dried. The samples were redissolved with 100 μL 80% methanol and stored at −80 °C prior to the LC–MS analysis. In addition, pooled QC samples were also prepared by combining 10 μL of each extraction mixture.

All samples were acquired by the LC–MS system, followed machine orders. Firstly, all chromatographic separations were performed using an UltiMate 3000 UPLC System (Thermo Fisher Scientific, Bremen, Germany). An ACQUITY UPLC T3 column (100 mm × 2.1 mm, 1.8 μm; Waters, Milford, MA, United States) was used for the reversed phase separation. The column oven was maintained at 35 °C. The flow rate was 0.4 mL/min and the mobile phase consisted of Solvent A (water, 0.1% formic acid) and Solvent B (acetonitrile, 0.1% formic acid). Gradient elution conditions were set as follows: 0 to 0.5 min, 5% B; 0.5 to 7 min, 5% to 100% B; 7 to 8 min, 100% B; 8 to 8.1 min, 100% to 5% B; 8.1 to 10 min, 5% B.

A high-resolution tandem mass spectrometer Q-Exactive (Thermo Scientific) was used to detect metabolites eluted from the column. The Q-Exactive was operated in both positive and negative ion modes. Precursor spectra (70 to 1,050 *m*/*z*) were collected at 70,000 resolution to hit an AGC target of 3e6. The maximum inject time was set to 100 ms. A top 3 configuration to acquire data was set in DDA mode. Fragment spectra were collected at 17,500 resolution to hit an AGC target of 1e5 with a maximum inject time of 80 ms. In order to evaluate the stability of the LC–MS during the whole acquisition, a QC sample (pool of all samples) was acquired after every 10 samples.

The acquired MS data were pretreated using various methods, including peak picking, peak grouping, retention time (RT) correction, second peak grouping, and annotation of isotopes and adducts. These pretreatments were performed using XCMS software. LC–MS raw data files were converted into mzXML format and then processed by the XCMS, CAMERA, and metaX toolbox implemented with the R software. Each ion was identified by combining RT and *m*/*z* data. The intensities of each peak were recorded, and a 3D matrix was generated, containing peak indices (RT *m*/*z* pairs), sample names (observations), and ion intensity information (variables).

Metabolites were annotated using the online KEGG database, by matching the exact molecular mass data (*m*/*z*) of samples with those in database. If the mass difference between the observed and the database value was <10 ppm, the metabolite was annotated. The molecular formula of metabolites was further identified and validated by the isotopic distribution measurements. Metabolite identification was also validated using an in-house fragment spectrum library. The intensity of peak data was further preprocessed by metaX. Features that were detected in <50% of QC samples or 80% of biological samples were removed; the remaining peaks with missing values were imputed using the *k*-nearest neighbor algorithm to improve the data quality. QC-based robust LOESS signal correction was fitted to the QC data to minimize signal intensity drift over time, considering the order of injection. Additionally, the relative SDS of the metabolic features were calculated across all QC samples, and those exceeding 30% were removed. Differences in metabolite concentrations between 2 samples were assessed using Student's *t*-test, assuming unequal variances.

Accession numbers

Sequence data from this article can be found in the GenBank/EMBL data libraries under accession numbers: AF525402 (*GmSOS2L*), NM_001250265 (*GmbZIP131*), and MH190223 (*GmICHG*).

Acknowledgments

The authors thank Professor Liwen Jiang from The Chinese University of Hong Kong and Professor Jinshan Gui from Zhejiang A&F University for their insightful comments and suggestions on earlier versions of this manuscript. They extend their gratitude to Professor Dajian Zhang from Shandong Agricultural University for his invaluable guidance on the generation of hairy roots.

Author contributions

E.P. was the originator of the overarching concept and was responsible for the design of the experiments. The manuscript was authored collaboratively by E.P., H.S., J.S., and S.W. The experimental procedures and data analysis were conducted with precision by X.N., Y.W., L.Da., K.J., S.Z., Y.H., Y.Z., L.Du., C.B., and Q.L.

Supplementary data

The following materials are available in the online version of this article.

Supplementary Figure S1. Evolutionary relationships within the bZIP transcription factor protein family.

Supplementary Figure S2. Transcriptional expression profile of *GmbZIP131*.

Supplementary Figure S3. GmbZIP131 enhances salinity tolerance in soybeans.

Supplementary Figure S4. QC assessment of MS-based proteomics data.

Supplementary Figure S5. Significance of flavonoid synthesis–related proteins in salt responses.

Supplementary Figure S6. PCA analysis for RNA-seq.

Supplementary Figure S7. Verification of GmbZIP131 protein localization in nuclear fractions by immunoblot analysis.

Supplementary Figure S8. Screening for transgenic soybean hairy roots with enhanced expression of *GmbZIP131* and *GmICHG*.

Supplementary Figure S9. Overview of metabolomics data acquisition by MS.

Supplementary Figure S10. Identification of transgenic soybean hairy roots with GmbZIP131 and GmSOS2L OE.

Supplementary Figure S11. GmbZIP131-mediated regulation of *GmICHG* potentiates salinity tolerance in soybeans.

Supplementary Figure S12. GmSOS2L specifically phosphorylates GmbZIP131 at S135 in vitro.

Supplementary Figure S13. DsRed-mediated screening of soybean hairy roots transformed with GmbZIP131$^{S135S/A/D}$ OE and GmbZIP131-RNAi constructs.

Supplementary Figure S14. Comprehensive analysis of differentially accumulated metabolites (DAMs) governed by GmSOS2L and GmICHG.

Supplementary Figure S15. KEGG enrichment bubble diagram and circle diagram revealing the accumulation of DAMs regulated by GmSOS2L.

Supplementary Figure S16. KEGG enrichment bubble diagram and circle diagram revealing the accumulation of DAMs regulated by GmICHG.

Supplementary Table S1. The detailed information of the proteome analysis in this study.

Supplementary Table S2. The quantitative data of proteins classified as flavonoids.

Supplementary Table S3. The data quality analysis of RNA-seq.

Supplementary Table S4. Reads alignment and statistical analysis of RNA-seq.

Supplementary Table S5. Grouping of RNA-sequencing samples.

Supplementary Table S6. Comprehensive transcriptomic profiling: an in-depth analysis of gene expression regulated by GmbZIP131 in this study. Due to the large size of this file, it has been divided into 2 parts, Supplementary Tables S6-1 and S6-2, for uploading.

Supplementary Table S7. Venn diagram intersection analysis: elucidating the core gene set dynamics.

Supplementary Table S8. Metabolomic insights: a detailed examination of metabolites regulated by GmbZIP131 in this study.

Supplementary Table S9. Quantitative metabolite profiling: differentially accumulated flavonoids regulated by GmbZIP131.

Supplementary Table S10. Quantitative analysis of differentially accumulated isoflavones regulated by GmbZIP131.

Supplementary Table S11. Proteomic dissection of phosphorylation events induced by salinity stress.

Supplementary Table S12. Metabolomic insights: a detailed examination of metabolites in hairy roots overexpressing GmSOS2L or GmICHG under salt stress conditions.

Supplementary Table S13. List of primer sequences used in this study.

Supplementary Table S14. Quantitative metabolite profiling: co-regulation of isoflavone in hairy roots by GmSOS2L and GmICHG under salt stress conditions.

Supplementary Table S15. Quantitative metabolite profiling: co-regulation of flavonoids in hairy roots by GmSOS2L and GmICHG under salt stress conditions.

Funding

This work was supported by grants from the National Natural Science Foundation of China (grant nos. 31970286 and 31301053), the Natural Science Foundation of Zhejiang Province (grant nos. LY22C020001, LY17C020004, and LR20C020001), the Hangzhou Joint Fund of the Zhejiang Provincial Natural Science Foundation of China (grant nos. LHZSZ24C010001 and LHZQN25C130006), the Hangzhou Science and Technology Bureau (grant no. 20170432B01), the Zhejiang Provincial Education Department (grant nos. JGBA2024428, JGBA2024811, and Y202351641), and the Zhejiang Provincial Science and Technology Department (grant no. 2025SDXT004-2).

Conflict of interest statement. The authors declared that they have no conflicts of interest to this work.

Data availability

All data are available in the main text and the Supplementary data.

References

Akagi T, Katayama-Ikegami A, Kobayashi S, Sato A, Kono A, Yonemori K. Seasonal abscisic acid signal and a basic leucine zipper transcription factor, DkbZIP5, regulate proanthocyanidin biosynthesis in persimmon fruit. *Plant Physiol*. 2012:158(2):1089–1102. https://doi.org/10.1104/pp.111.191205

Alvarez-Rivera G, Sanz A, Cifuentes A, Ibánez E, Paape T, Lucas MM, Pueyo JJ. Flavonoid accumulation varies in *Medicago truncatula* in response to mercury stress. *Front Plant Sci*. 2022:3:933209. https://doi.org/10.3389/fpls.2022.933209

An JP, Qu FJ, Yao JF, Wang XN, You CX, Wang XF, Hao YJ. The bZIP transcription factor MdHY5 regulates anthocyanin accumulation and nitrate assimilation in apple. *Hortic Res*. 2017:4(1):17023. https://doi.org/10.1038/hortres.2017.23

Babbar R, Karpinska B, Grover A, Foyer CH. Heat-induced oxidation of the nuclei and cytosol. *Front Plant Sci*. 2021:11:617779. https://doi.org/10.3389/fpls.2020.617779

Chen H, Zou Y, Shang Y, Lin H, Wang Y, Cai R, Tang X, Zhou JM. Firefly luciferase complementation imaging assay for protein-protein interactions in plants. *Plant Physiol*. 2008:146(2):368–376. https://doi.org/10.1104/pp.107.111740

Dash M, Yordanov YS, Georgieva T, Tschaplinski TJ, Yordanova E, Busov V. Poplar PtabZIP1-like enhances lateral root formation and biomass growth under drought stress. *Plant J*. 2017:9(4):692–705. https://doi.org/10.1111/tpj.13413

Du WM, Lin HX, Chen S, Wu YS, Zhang J, Fuglsang AT, Palmgren MG, Wu WH, Guo Y. Phosphorylation of SOS3-like calcium-binding proteins by their interacting SOS2-like protein kinases is a common regulatory mechanism in Arabidopsis. *Plant Physiol*. 2011:156(4):2235–2243. https://doi.org/10.1104/pp.111.173377

Erasto P, Bojase-Moleta G, Majinda RRT. Antimicrobial and antioxidant flavonoids from the root wood of *Bolusanthus speciosus*. *Phytochemistry*. 2004:65(7):875–880. https://doi.org/10.1016/j.phytochem.2004.02.011

Feng Y, Wang Y, Zhang GF, Gan ZY, Gao M, Lv JH, Wu T, Zhang XZ, Xu XF, Yang SH, *et al.* Group-C/S1 bZIP heterodimers regulate to negatively modulate drought tolerance in apple species. *Plant J*. 2021:107(2):399–417. https://doi.org/10.1111/tpj.15296

Ferreyra MLF, Rius SP, Casati P. Flavonoids: biosynthesis, biological functions, and biotechnological applications. *Front Plant Sci*. 2012:3:222. https://doi.org/10.3389/fpls.2012.00222

Gallé A, Bela K, Hajnal A, Faragó N, Horváth E, Horváth M, Puskás L, Csiszár J. Crosstalk between the redox signalling and the detoxification: GSTs under redox control? *Plant Physiol Biochem*. 2021:169:149–159. https://doi.org/10.1016/j.plaphy.2021.11.009

Gani U, Vishwakarma RA, Misra P. Membrane transporters: the key drivers of transport of secondary metabolites in plants. *Plant Cell Rep*. 2021:40(1):1–18. https://doi.org/10.1007/s00299-020-02599-9

Gao SQ, Chen M, Xu ZS, Zhao CP, Li LC, Xu HJ, Tang YM, Zhao X, Ma YZ. The soybean GmbZIP1 transcription factor enhances multiple abiotic stress tolerances in transgenic plants. *Plant Mol Biol*. 2011:75(6):537–553. https://doi.org/10.1007/s11103-011-9738-4

Gao Z, Chen Z, Cui Y, Ke M, Xu H, Xu Q, Chen J, Li Y, Huang L, Zhao H, *et al.* GmPIN-dependent polar auxin transport is involved in soybean nodule development. *Plant Cell*. 2021:33(9):2981–3003. https://doi.org/10.1093/plcell/koab183

Gong DM, Guo Y, Jagendorf AT, Zhu JK. Biochemical characterization of the Arabidopsis protein kinase SOS2 that functions in salt tolerance. *Plant Physiol*. 2002:130(1):256–264. https://doi.org/10.1104/pp.004507

Hao R, Zhou W, Li J, Luo M, Scheres B, Guo Y. On salt stress, PLETHORA signaling maintains root meristems. *Dev Cell*. 2023:58(18):1657–1669.e5. https://doi.org/10.1016/j.devcel.2023.06.012

Hartmann U, Sagasser M, Mehrtens F, Stracke R, Weisshaar B. Differential combinatorial interactions of *cis*-acting elements recognized by R2R3-MYB, bZIP, and bHLH factors control light-responsive and tissue-specific activation of phenylpropanoid biosynthesis genes. *Plant Mol Biol*. 2005:57(2):155–171. https://doi.org/10.1007/s11103-004-6910-0

Hassani D, Fu X, Shen Q, Khalid M, Rose JKC, Tang K. Parallel transcriptional regulation of artemisinin and flavonoid biosynthesis. *Trends Plant Sci*. 2020:25(5):466–476. https://doi.org/10.1016/j.tplants.2020.01.001

Huang XS, Wang W, Zhang Q, Liu JH. A basic helix-loop-helix transcription factor, PtrbHLH, of *Poncirus trifoliata* confers cold tolerance and modulates peroxidase-mediated scavenging of hydrogen peroxide. *Plant Physiol*. 2013:162(2):1178–1194. https://doi.org/10.1104/pp.112.210740

Jakoby M, Weisshaar B, Dröge-Laser W, Vicente-Carbajosa J, Tiedemann J, Kroj T, Parcy F; bZIP Research Group. bZIP transcription factors in Arabidopsis. *Trends Plant Sci*. 2002:7(3):106–111. https://doi.org/10.1016/S1360-1385(01)02223-3

Jiang RR, Zhou SC, Da X, Yan P, Wang K, Xu JM, Mo XR. OsMKK6 regulates disease resistance in rice. *Int J Mol Sci*. 2023:24(16):12678. https://doi.org/10.3390/ijms241612678

Kader MA, Lindberg S. Cytosolic calcium and pH signaling in plants under salinity stress. *Plant Signal Behav*. 2010:5(3):233–238. https://doi.org/10.4161/psb.5.3.10740

Kadota Y, Sklenar J, Derbyshire P, Stransfeld L, Asai S, Ntoukakis V, Jones J, Shirasu K, Menke F, Jones A, *et al.* Regulation of the NADPH oxidase RBOHD by the PRR-associated kinase BIK1 during plant immunity. *Mol Cell*. 2014:54(1):43–55. https://doi.org/10.1016/j.molcel.2014.02.021

Katiyar-Agarwal S, Zhu J, Kim K, Agarwal M, Fu X, Huang A, Zhu JK. The plasma membrane Na^+/H^+ antiporter SOS1 interacts with RCD1 and functions in oxidative stress tolerance in Arabidopsis. *Proc Natl Acad Sci U S A*. 2006:103(49):18816–18821. https://doi.org/10.1073/pnas.0604711103

Kereszt FA, Li DX, Indrasumunar A, Nguyen CDT, Nontachaiyapoom S, Kinkema M, Gresshoff PM. *Agrobacterium rhizogenes*–mediated transformation of soybean to study root biology. *Nat Protoc*. 2007:2(4):948–952. https://doi.org/10.1038/nprot.2007.141

Ketehouli T, Zhou YG, Dai SY, Carther KFI, Sun DQ, Li Y, Nguyen QVH, Xu H, Wang FW, Liu WC, *et al.* A soybean calcineurin B-like protein-interacting protein kinase, GmPKS4, regulates plant responses to salt and alkali stresses. *J Plant Physiol*. 2021:256:153331. https://doi.org/10.1016/j.jplph.2020.153331

Kim D, Langmead B, Salzberg SL. HISAT: a fast spliced aligner with low memory requirements. *Nat Methods*. 2015:12(4):357–360. https://doi.org/10.1038/NMETH.3317

Kumar S, Awana M, Rani K, Kumari S, Sasi M, Dahuja A. Soybean (*Glycine max*) isoflavone conjugate hydrolysing β-glucosidase (GmICHG): a promising candidate for soy isoflavone bioavailability enhancement. *3 Biotech*. 2023:13(2):52. https://doi.org/10.1007/s13205-022-03427-5

Li C, Wu J, Hu KD, Wei SW, Sun HY, Hu LY, Han Z, Yao GF, Zhang H. PyWRKY26 and PybHLH3 cotargeted the *PyMYB114* promoter to regulate anthocyanin biosynthesis and transport in red-skinned pears. *Hortic Res*. 2020:7(1):37. https://doi.org/10.1038/s41438-020-0254-z

Li Q, Fu H, Yu X, Wen X, Guo H, Guo Y, Li J. The SOS2-CTR1 module coordinates plant growth and salt tolerance in Arabidopsis. *Exp Bot*. 2024:75(1):391–404. https://doi.org/10.1093/jxb/erad368

Liu JX, Srivastava R, Howell SH. Stress-induced expression of an activated form of AtbZIP17 provides protection from salt stress in *Arabidopsis*. *Plant Cell Environ*. 2008:31(12):1735–1743. https://doi.org/10.1111/j.1365-3040.2008.01873.x

Liu SL, Zhang M, Feng F, Tian ZX. Toward a "green revolution" for soybean. *Mol Plant*. 2020:13(5):688–697. https://doi.org/10.1016/j.molp.2020.03.002

Liu XN, Yu X, Shi Y, Ma L, Fu Y, Guo Y. Phosphorylation of RhoGDI1, a Rho GDP dissociation inhibitor, regulates root hair development in *Arabidopsis* under salt stress. *Proc Natl Acad Sci U S A*. 2023:120(34):e217957120. https://doi.org/10.1073/pnas.2217957120

Liu YK, He CZ. Regulation of plant reactive oxygen species (ROS) in stress responses: learning from AtRBOHD. *Plant Cell Rep*. 2016:35(5):995–1007. https://doi.org/10.1007/s00299-016-1950-x

Livak KJ, Schmittgen TD. Analysis of relative gene expression data using real-time quantitative PCR and the 2(-delta delta C(T)) method. *Methods*. 2001:25(4):402–408. https://doi.org/10.1006/meth.2001.1262

Luan S, Kudla J, Rodriguez-Concepcion M, Yalovsky S, Gruissem W. Calmodulins and calcineurin B-like proteins: calcium sensors for specific signal response coupling in plants. *Plant Cell*. 2002:14(Suppl. 1):S389–S400. https://doi.org/10.1105/tpc.001115

Ma S, Niu H, Liu C, Zhang J, Hou C, Wang D. Expression stabilities of candidate reference genes for RT-qPCR under different stress conditions in soybean. *PLoS One*. 2013:8(10):e75271. https://doi.org/10.1371/journal.pone.0075271

Malacarne G, Coller E, Czemmel S, Vrhovsek U, Engelen K, Goremykin V, Bogs J, Moser C. The grapevine VvibZIPC22 transcription factor is involved in the regulation of flavonoid biosynthesis. *J Exp Bot*. 2016:67(11):3509–3522. https://doi.org/10.1093/jxb/erw181

Mao X, Cai T, Olyarchuk JG, Wei L. Automated genome annotation and pathway identification using the KEGG orthology (KO) as a controlled vocabulary. *Bioinformatics*. 2005:21(19):3787–3793. https://doi.org/10.1093/bioinformatics/bti430

Matsuda H, Yamazaki Y, Moriyoshi E, Nakayasu M, Yamazaki S, AokiY, Takase H, Okazaki S, Nagano AJ, Kaga A, *et al.* Apoplast-localized beta-glucosidase elevates isoflavone accumulation in the soybean rhizosphere. *Plant Cell Physiol*. 2023:64(5):486–500. https://doi.org/10.1093/pcp/pcad012

Mittler R. ROS are good. *Trends Plant Sci*. 2017:22(1):11–19. https://doi.org/10.1016/j.tplants.2016.08.002

Mittler R, Zandalinas S, Fichman Y, Breusegem F. Reactive oxygen species signalling in plant stress responses. *Nat Rev Mol Cell Bio*. 2022:23(10):663–679. https://doi.org/10.1038/s41580-022-00499-2

Møller IM, Jensen PE, Hansson A. Oxidative modifications to cellular components in plants. *Annu Rev Plant Biol*. 2007:58(1):459–481. https://doi.org/10.1146/annurev.arplant.58.032806.103946

Muhlemann JK, Younts TLB, Muday GK. Flavonols control pollen tube growth and integrity by regulating ROS homeostasis during high-temperature stress. *Proc Natl Acad Sci U S A*. 2018:115(47):E11188–E11197. https://doi.org/10.1073/pnas.1811492115

Munns R, Tester M. Mechanisms of salinity tolerance. *Annu Rev Plant Biol*. 2008:59(1):651–681. https://doi.org/10.1146/annurev.arplant.59.032607.092911

Ohta M, Guo Y, Halfter U, Zhu JK. A novel domain in the protein kinase SOS2 mediates interaction with the protein phosphatase 2C ABI2. *Proc Natl Acad Sci U S A*. 2003:100(20):11771–11776. https://doi.org/10.1073/pnas.2034853100

Pi E, Xu J, Li HH, Fan W, Zhu CM, Zhang TY, Jiang JC, He LT, Lu HF, Wang HZ, *et al*. Enhanced salt tolerance of rhizobia-inoculated soybean correlates with decreased phosphorylation of the transcription factor GmMYB183 and altered flavonoid biosynthesis. *Mol Cell Proteomics*. 2019:18(11):2225–2243. https://doi.org/10.1074/mcp.RA119.001704

Pi E, Zhu C, Fan W, Huang Y, Qu L, Li Y, Zhao Q, Ding F, Qiu L, Wang H, *et al*. Quantitative phosphoproteomic and metabolomic analyses reveal GmMYB173 optimizes flavonoid metabolism in soybean under salt stress. *Mol Cell Proteomics*. 2018:17(6):1209–1224. https://doi.org/10.1074/mcp.RA117.000417

Rasheed A, Raza A, Jie HD, Mahmood A, Ma YS, Zhao L, Xing HC, Li LL, Hassan MU, Qari SH, *et al*. Molecular tools and their applications in developing salt-tolerant soybean (*Glycine max* L.) cultivars. *Bioengineering (Basel)*. 2022:9(10):495. https://doi.org/10.3390/bioengineering9100495

Ren J, Huang QH, Xu YY, Yang M, Yang J, Hu K. Isoflavone lupiwighteone induces cytotoxic, apoptotic, and antiangiogenic activities in DU-145 prostate cancer cells. *Anticancer Drugs*. 2015:26(6):599–611. https://doi.org/10.1097/Cad.0000000000000224

Ren YR, Zhao Q, Yang YY, Zhang R, Wang XF, Zhang TE, You CX, HuoHQ, Hao YJ. Interaction of BTB-TAZ protein MdBT2 and DELLA protein MdRGL3a regulates nitrate-mediated plant growth. *Plant Physiol*. 2021:186(1):750–766. https://doi.org/10.1093/plphys/kiab065

Rolly NK, Imran QM, Lee IJ, Yun BW. Salinity stress-mediated suppression of expression of salt overly sensitive signaling pathway genes suggests negative regulation by AtbZIP62 transcription factor in *Arabidopsis thaliana*. *Int J Mol Sci*. 2020:21(5):1726. https://doi.org/10.3390/ijms21051726

Shapiguzov A, Vainonen JP, Wrzaczek M, Kangasjärvi J. ROS-talk—how the apoplast, the chloroplast, and the nucleus get the message through. *Front Plant Sci*. 2012:3:292. https://doi.org/10.3389/fpls.2012.00292

Shen J, Zhao R. Live measurement of organelle pH by plant pHluorins. *Trends Plant Sci*. 2023:28(4):486–487. https://doi.org/10.1016/j.tplants.2022.12.009

Song Z, Yang Q, Dong B, Li N, Wang M, Du T, Liu N, Niu L, Jin H, Meng D, *et al*. Melatonin enhances stress tolerance in pigeon pea by promoting flavonoid enrichment, particularly luteolin in response to salt stress. *J Exp Bot*. 2022:73(17):5992–6008. https://doi.org/10.1093/jxb/erac276

Sugiyama A, Shitan N, Yazaki K. Involvement of a soybean ATP-binding cassette-type transporter in the secretion of genistein, a signal flavonoid in legume-rhizobium symbiosis. *Plant Physiol*. 2007:144(4):2000–2008. https://doi.org/10.1104/pp.107.096727

Suzuki H, Takahashi S, Watanabe R, Fukushima Y, Fujita N, Noguchi A, Yokoyama R, Nishitani K, Nishino T, Nakayama T. An isoflavone conjugate-hydrolyzing β-glucosidase from the roots of soybean (*Glycine max*) seedlings. *J Biol Chem*. 2006:281(40):30251–30259. https://doi.org/10.1074/jbc.M605726200

Suzuki N, Miller G, Salazar C, Mondal HA, Shulaev E, Cortes DF, Shuman JL, Luo XZ, Shah J, Schlauch K, *et al*. Temporal-spatial interaction between reactive oxygen species and abscisic acid regulates rapid systemic acclimation in plants. *Plant Cell*. 2013:25(9):3553–3569. https://doi.org/10.1105/tpc.113.114595

Takagi D, Takumi S, Hashiguchi M, Sejima T, Miyake C. Superoxide and singlet oxygen produced within the thylakoid membranes both cause photosystem I photoinhibition. *Plant Physiol*. 2016:171(3):1626–1634. https://doi.org/10.1104/pp.16.00246

Tang W, Page M, Fei YJ, Liu LC, Xu F, Cai XD, Yuan LY, Wu QS, ZhouMQ. Overexpression of *AtbZIP60deltaC* gene alleviates salt-induced oxidative damage in transgenic cell cultures. *Plant Mol Biol Rep*. 2012:30(5):1183–1195. https://doi.org/10.1007/s11105-012-0437-3

Trapnell C, Williams BA, Pertea G, Mortazavi A, Kwan G, van Baren MJ, Salzberg SL, Wold BJ, Pachter L. Transcript assembly and quantification by RNA-Seq reveals unannotated transcripts and isoform switching during cell differentiation. *Nat Biotechnol*. 2010:28(5):511–515. https://doi.org/10.1038/nbt.1621

Vadivel AKA, McDowell T, Renaud JB, Dhaubhadel S. A combinatorial action of GmMYB176 and GmbZIP5 controls isoflavonoid biosynthesis in soybean (*Glycine max*). *Commun Biol*. 2021:4(1):356. https://doi.org/10.1038/s42003-021-01889-6

Van Leene J, Blomme J, Kulkarni SR, Cannoot B, De Winne N, Eeckhout D, Persiau G, Van De Slijke E, Vercruysse L, Bossche RV, *et al*. Functional characterization of the Arabidopsis transcription factor bZIP29 reveals its role in leaf and root development. *J Exp Bot*. 2016:67(19):5825–5840. https://doi.org/10.1093/jxb/erw347

van Zelm E, Zhang YX, Testerink C. Salt tolerance mechanisms of plants. *Annu Rev Plant Biol*. 2020:71(1):403–433. https://doi.org/10.1146/annurev-arplant-050718-100005

Verslues PE, Batelli G, Grillo S, Agius F, Kim YS, Zhu J, Agarwal M, Katiyar-Agarwal S, Zhu JK. Interaction of SOS2 with nucleoside diphosphate kinase 2 and catalases reveals a point of connection between salt stress and H_2O_2 signaling in *Arabidopsis thaliana*. *Mol Cell Biol*. 2007:27(22):7771–7780. https://doi.org/10.1128/MCB.00429-07

Wang J, Hou Q, Li P, Yang L, Sun X, Benedito VA, Wen J, Chen B, Mysore KS, Zhao J. Diverse functions of multidrug and toxin extrusion (MATE) transporters in citric acid efflux and metal homeostasis in *Medicago truncatula*. *Plant J*. 2017:90(1):79–95. https://doi.org/10.1111/tpj.13471

Wang N, Liu WJ, Yu L, Guo ZW, Chen ZJ, Jiang SH, Xu HF, Fang HC, Wang YC, Zhang ZY, *et al*. HEAT SHOCK FACTOR A8a modulates flavonoid synthesis and drought tolerance. *Plant Physiol*. 2020:184(3):1273–1290. https://doi.org/10.1104/pp.20.01106

Wang T, Guo J, Peng Y, Lyu X, Liu B, Sun S, Wang X. Light-induced mobile factors from shoots regulate rhizobium-triggered soybean root nodulation. *Science*. 2021:374(6563):65–71. https://doi.org/10.1126/science.abh2890

Wang YC, Gao CQ, Liang YN, Wang C, Yang CP, Liu GF. A novel bZIP gene from *Tamarix hispida* mediates physiological responses to salt stress in tobacco plants. *Plant Physiol*. 2010:167(3):222–230. https://doi.org/10.1016/j.jplph.2009.09.008

Yan JH, Wang BA, Jiang YN, Cheng LJ, Wu TL. GmFNSII-controlled soybean flavone metabolism responds to abiotic stresses and regulates plant salt tolerance. *Plant Cell Physiol*. 2014:55(1):74–86. https://doi.org/10.1093/pcp/pct159

Yang O, Popova OV, Süthoff U, Lüking I, Dietz KJ, Golldack D. The *Arabidopsis* basic leucine zipper transcription factor AtbZIP24 regulates complex transcriptional networks involved in abiotic stress resistance. *Gene*. 2009:436(1–2):45–55. https://doi.org/10.1016/j.gene.2009.02.010

Yang Y, Yu TF, Ma J, Chen J, Zhou YB, Chen M, Ma YZ, Wei WL, Xu ZS. The soybean bZIP transcription factor gene *GmbZIP2* confers drought and salt resistances in transgenic plants. *Int J Mol Sci*. 2020:21(2):670. https://doi.org/10.3390/ijms21020670

Yu Y, Qian YC, Jiang MY, Xu J, Yang JT, Zhang TY, Gou LP, Pi EX. Regulation mechanisms of plant basic leucine zippers to various

abiotic stresses. *Front Plant Sci*. 2020:11:1258. https://doi.org/10.3389/fpls.2020.01258

Zhang C, Shao Z, Kong Y, Du H, Li W, Yang Z, Li X, Ke H, Sun Z, Shao J, *et al*. High-quality genome of a modern soybean cultivar and resequencing of 547 accessions provide insights into the role of structural variation. *Nat Genet*. 2024:56(10):2247–2258. https://doi.org/10.1038/s41588-024-01901-9

Zhou F, Lin QB, Zhu LH, Ren YL, Zhou KN, Shabek N, Wu FQ, Mao HB, Dong W, Gan L, *et al*. D14–SCF^{D3}-dependent degradation of D53 regulates strigolactone signaling. *Nature*. 2013:504(7480):406–410. https://doi.org/10.1038/nature12878

Zhou H, Lin HX, Chen S, Becker K, Yang YQ, Zhao JF, Kudla J, Schumaker KS, Guo Y. Inhibition of the Arabidopsis salt overly sensitive pathway by 14-3-3 proteins. *Plant Cell*. 2014:26(3):1166–1182. https://doi.org/10.1105/tpc.113.117069

Zhu J, Fu X, Koo YD, Zhu JK, Jenney FE Jr, Adams MW, Zhu Y, Shi H, Yun DJ, Hasegawa PM, *et al*. An enhancer mutant of Arabidopsis salt overly sensitive 3 mediates both ion homeostasis and the oxidative stress response. *Mol Cell Biol*. 2007:27(14):5214–5224. https://doi.org/10.1128/MCB.01989-06

Zhu JK. Abiotic stress signaling and responses in plants. *Cell*. 2016:167(2):313–324. https://doi.org/10.1016/j.cell.2016.08.029